ISTANBUL TECHNICAL UNIVERSITY ★ GRADUATE SCHOOL OF SCIENCE ENGINEERING AND TECHNOLOGY

GRAPHENE OXIDE FIBERS, PRODUCTION, CHARACTERIZATION AND UTILIZATION ON THE ADSORPTION OF SULFUR DIOXIDE

M.Sc. THESIS

Özge ALPTOĞA

Polymer Science and Technology Department
Polymer Science and Technology Programme

DECEMBER 2017

ISTANBUL TECHNICAL UNIVERSITY ★ GRADUATE SCHOOL OF SCIENCE ENGINEERING AND TECHNOLOGY

GRAPHENE OXIDE FIBERS, PRODUCTION, CHARACTERIZATION AND UTILIZATION ON THE ADSORPTION OF SULFUR DIOXIDE

M.Sc. THESIS

Özge ALPTOĞA
(515151037)

Polymer Science and Technology Department

Polymer Science and Technology Programme

Thesis Advisor: Prof. Dr. Hacer Ayşen ÖNEN

DECEMBER 2017

ISTANBUL TEKNİK ÜNİVERSİTESİ ★ FEN BİLİMLERİ ENSTİTÜSÜ

GRAFEN OKSİT LİFLERİ, ÜRETİMİ, KARAKTERİZASYONU VE KÜKÜRT DİOKSİT ADSORPSİYONUNDA KULLANIMI

YÜKSEK LİSANS TEZİ

Özge ALPTOĞA
(515151037)

Polimer Bilimi ve Teknolojisi Anabilim Dalı

Polimer Bilimi ve Teknolojisi Programı

Tez Danışmanı: Prof. Dr. Hacer Ayşen ÖNEN

ARALIK 2017

Özge ALPTOĞA, a M.Sc.student of İTU Graduate School of Science Engineering and Technology student ID 515151037, successfully defended the thesis entitled "GRAPHENE OXIDE FIBERS, PRODUCTION, CHARACTERIZATION AND UTILIZATION ON THE ADSORPTION OF SULFUR DIOXIDE", which she prepared after fulfilling the requirements specified in the associated legislations, before the jury whose signatures are below.

Thesis Advisor :	**Prof. Dr. Hacer Ayşen ÖNEN** Istanbul Technical University	.....
Jury Members :	**Prof. Dr. Nuray UÇAR** Istanbul Technical University	.....
	Prof. Dr. Ayfer SARAÇ Yıldız Technical University	.....

Date of Submission : 17 November 2017
Date of Defense : 14 December 2017

To my beloved mother,

FOREWORD

My most sincere thanks to my supervisors Professor Dr. Ayşen Önen, Professor Dr. Nuray Uçar and Professor Dr. Nilgün Yavuz for their encouragement, personal guidance, assistance and valuable suggestions enabling me to steer my research work efficiently and effectively. Their wide knowledge and logical approach had been extremely useful for my research work.

My special thanks go to my laboratory colleague Mervin Ölmez for her friendship and kind supports.

I am grateful of the financial supports and scholarships from The Scientific And Technological Research Council of Turkey (TUBITAK) (Project No: 114M524) and İstanbul Technical University Scientific Research Projects Coordination Unit (İTU BAP) (Project ID: 40709).

I extend my sincere appreciation and love to my parents, my workmates, and friends for their great love, support, and understanding.

Last in this list but first in my heart are my beloved family members especially my mother. I wish to express my warmest gratitude to you for giving me endless support, love, caring and happiness.

December 2017

Özge ALPTOĞA
(Chemical Engineer)

TABLE OF CONTENTS

Page

ABBREVIATIONS

AC	:Activated carbon
AFM	:Atomic Force Microscopy
APS	:Average Particle Size
C	:Carbon
$CaCl_2$	:Calcium chloride
cm	:Cantimeter
CV	:Coefficient of variation
D	:Dimension
EDS	:Energy-dispersive X-ray Spectroscopy
FTIR	:Fourier Transform Infrared Spectroscopy
g	:Gram
GO	:Graphene oxide
h	:Hour
HCl	:Hydrochloric acid
H_2O_2	:Hydrogen peroxide
H_2SO_4	:Sulfuric acid
kg	:Kilogram
$KMnO_4$	:Potassium permanganate
kV	:Kilovolt
mg	:Miligram
min	:Minute
mL	:Mililiter
mm	:Milimeter
$NaNO_3$	:Sodium nitrate
NaOH	:Sodium hydroxide
nm	:Nanometer
rpm	:Revolutions per minute
SEM	:Scanning Electron Microscopy
SLPM	:Standard liter per minute
SO_2	:Sulfurdioxide
Std	:Standart Sapma
XRD	:X-ray Diffraction

SYMBOLS

Å	:Angstrom
µm	:Mikrometer
wt	:Weight
t	:Time
S	:Siemens
sec	:Second

LIST OF TABLES

Page

LIST OF FIGURES

Page

GRAPHENE OXIDE FIBERS, PRODUCTION, CHARACTERIZATION AND UTILIZATION ON THE ADSORPTION OF SULFUR DIOXIDE

SUMMARY

Fossil fuel combustion and other industrial activities cause the emission of sulfur dioxide (SO_2) gas. SO_2 is an air pollutant gas and a very toxic for human health and nature. Hence, cleaning of this harmful gas is an important issue. Graphene which is two-dimensional material has excellent mechanical, chemical, thermal properties, and many application areas such as energy storage devices, gas adsorption, sensing devices, and optical electronics. Further, graphene oxide (GO) is examined as a good adsorbent because of its important features such as functional groups (epoxy, carboxyl and hydroxyl) on the surface and layered structure. As a fiber form, the SO_2 adsorption properties of the fibers are usually investigated on carbon fibers.

This thesis seeks to investigate the adsorption capabilities of graphene oxide fibers. For this purpose, graphene oxide was produced primarily by Hummers method and graphene oxide fiber were synthesized by the wet spinning method.To see the different effects, reduction process by hydrazine hydrate, activated carbon addition, poly(vinyl) alcohol (PVA) coating and single coagulation bath application were tried on GO fibers. Monitoring of the morphology of GO fibers was carried out by SEM and AFM, also other qualitative and quantitative analyses like XRD, FTIR, Raman, conductivity and tex number were performed. TGA was used characterize the thermal properties of fibers and most importantly the surface areas of fibers were calculated by BET analysis.It has been seen that process parameters such as dispersion preparation method, pH value of dispersion, the content of coagulation bath, reduction process, and additional materials affect the final properties of graphene oxide fiber.

Nonwoven based structure produced by GO fibers has an SO_2 adsorption capacity itself, approximately 310-320 mg SO_2/1 g of sample. However nonwoven structure produced by activated carbon doped GO fiber has 3 times higher SO_2 adsorption capacity than reference GO fiber. In accordance with adsorption capacity results, activated carbon doped sample has higher BET surface area.

GRAFEN OKSİT LİFLER, ÜRETİMİ, KARAKTERİZASYONU VE KÜKÜRT DİOKSİT ADSORPSİYONUNDA KULLANIMI

ÖZET

Karbon ve karbon bazlı malzemeler doğada çok önemli bir rol oynamaktadır ve diğer allotroplarından farklı olarak iki boyutlu formu grafendir. Grafen karbon atomlarının sp^2 hibritleşmesi sonucunda oluşmuştur. İlk olarak 2004 yılında grafitten mekanik olarak elde edilmiştir ve bu çalışma ile Manchester Üniversitesi'nden Andre Geim ve Konstantin Novoselov'a Nobel ödülü kazandırmıştır. Fullerenler ve karbon nanotüpler, grafen tabakasının, sırasıyla, küresel ve silindirik şekilde katlanmasıyla oluşur.

Karbon nanotüplerden farklı olarak grafen daha geniş spesifik yüzey alanına sahip olup, üretim maliyeti karbon nanotüplerinkinden daha düşüktür. Oldukça ince bir malzemedir, son derece yüksek mukavemete, termal iletkenlik ve elektrik iletkenliğine sahiptir. Enerji depolama, sensör, katalizör, adsorpsiyon vb. pek çok alanda kullanımı araştırılmaktadır.

Grafen oksit (GO), grafenin yüzeyinde oksijenli fonksiyonel gruplar ile bezenmesi ile oluşur.Grafen oksit eldesinde kullanılan en yaygın prosedür, öncesinde termal eksfoliasyona tabi tutulan grafit partiküllerinin oksidasyonudur. En eski ve en yaygın kullanılan proseslerden biri ise Hummers metodudur.Ayrıca grafit oksitin tek tabakalı hali olarak da adlandırılabilir. GO yapısında oksijen atomları karbonlara kovalent bağlarla bağlanmıştır ve hidroksil, epoksi ve karboksil fonksiyonel grupları bulunmaktadır. Bu gruplar sayesinde su veya diğer organik çözücüler içerisinde kolayca çözünebilmektedir.

Grafen oksitin tek tabakalı yapısı ve fonksiyonel grupları gazların (NH_3, SO_2, H_2S) adsorpsiyonunda etkin rol oynamaktadır. Bu çalışma kapsamında oldukça zararlı bir gaz olan kükürt dioksit (SO_2) gazının adsorpsiyonu araştırılmıştır.

Kükürt dioksit renksiz, kötü kokulu ve reaktif bir gazdır. Fosil yakıt kullanımı ve diğer endüstriyel faaliyetler veya volkanlar, orman yangını gibi doğa olayları kükürt dioksit (SO_2) gazı emisyonuna neden olur. SO_2 hava kirletici bir gazdır ve insan sağlığı ve doğa için oldukça toksiktir. Sera etkisine ve fotokimyasal dumana neden olur, oksijen ve su ile birleştiğinde ise sülfürik asit oluşturur ve asit yağmurlarını tetikler. Bu nedenle, bu zararlı gazın temizlenmesi önemli bir konudur. Önceki çalışmalar incelendiğinde, karbon bazlı malzemelerin adsorpsiyon uygulamalarının yoğun bir şekilde araştırıldığı görülmektedir. Ancak liflerin adsorpsiyon kapasitesi araştırmaları aktif karbon lifleri üzerine yapılmıştır. Bu tez çalışmasında ise grafen oksit liflerinin kükürt dioksit adsorpsiyon kapasitesi araştırılmıştır.

Çalışma 3 temel aşamadan oluşmaktadır. İlk aşamasında, Hummers metodu ile grafen oksit dispersionu elde edilmiştir. Yüksek adsorplama kapaitesine sahip olduğu bilinen aktif karbonun eklemesi de dispersiyona katılmasıyla sağlanmıştır. Katkısız dispersiyondan 3 banyolu, tek banyolu ve polivinil alkol (PVA) içerikli banyodan geçirilmiş grafen oksit lifleri üretilmiştir. Bu üretim sistemi yaş çekim (wet spinning)

metodu olarak adlandırılmaktadır.Ayrıca çeşitli indirgeme metotlarıyla indirgenmiş grafen oksit liflerinin ve indirgenmemiş grafen oksit liflerinin özellikleri incelenmek üzere üretilmiştir.

Çalışmanın ikinci aşaması, üretilen liflerin yapısı, karakterizasyonu, morfolojisi ve kristalinitesi gibi bilgileri elde etmek ve birbirleri ve literatür çalışmalarıyla karşılaştırmayı içermektedir.

Üçüncü aşamada ise adsorpsiyon kapasitesilerini ölçmek için grafen oksit lifleri ile dokunmamış tekstil yüzeyleri elde edilmiş ve bu dokunmamış yüzeylerin SO_2 gazını adsorbe etme özelliği olduğu gösterilmiştir.

GO liflerinin morfolojisinin izlenmesi SEM ve AFM testleri ile gerçekleştirilmiş, ayrıca XRD, FTIR, Raman, iletkenlik ve tex sayısı gibi diğer analizler yapılmıştır. TGA, liflerin termal özelliklerini karakterize etmek için kullanılmış ve liflerin yüzey alanları BET analizi ile hesaplanmıştır. Dispersiyon hazırlama yöntemi, dispersiyonun pH değeri, koagülasyon banyosu içeriği, indirgeme işlemi ve ilave malzemeler gibi işlem parametrelerinin, grafen oksit elyafının nihai özelliklerini etkilediği görülmüştür.

SEM analizlerinde aktif karbon, PVA katkılarıve tek banyo nedeniyle yüzeyde kalan $CaCl_2$ tuzları net bir şekilde gözlenmiştir. XRD analizi sonucunda kristal yapılar incelenmiş, her örnek için karakteristik pikler gözlenebilmiştir. Aynı şekilde FTIR ve Raman analizleri indirgeme, aktif karbon eklenmesi ve PVA kaplanması sonucu yeni pik oluşumu veya indirgemede olduğu gibi piklerin kaybolması ile işlemlerin doğru şekilde ilerlediğini ispat etmiştir. Hidrazin hidratla indirgemede yapıda oluşan defektler Raman analizinden elde edilen I_D/I_G değerinden ve SEM analizi görüntülerinden açıkça anlaşılmaktadır. PVA ise defektleri ve boşlukları kapatmıştır. En iletken malzeme, tek banyoya tabi tutulan grafen oksit lifleri olmuştur. TGA analizinin öncelikli amacı, BET analizi öncesi fonksiyonel grup kaybı olmadan çıkılabilecek enuygun degaz sıcaklığını bulmaktır. Buradan hareketle yapılan BET analizi sonuçlarında en yüksek yüzey alanı, ortalama gözenek çapı ve toplam gözenek hacmi değerleri, aktif karbon eklenmiş dispersiyondan elde edilen liflerde hesaplanmıştır.

GO lifleri tarafından üretilen dokunmamış yüzeylerin üzerinden öncelikle SO_2 gazı geçirilmiştir, sonrasında yüksek sıcaklıkta adsorbe edilen gaz çözelti içine hapsedilerek titrasyon hesaplaması ile adsorbe edilen gaz miktarı hesaplanmıştır. Katkısız liflerden üretilen dokunmamış yüzey, pH 3 ve pH 5 değerlerinde olduça yakın değerlerde (yaklaşık 310-320 mg SO_2 / 1 g örnek) SO_2 adsorpsiyon kapasitesine sahiptir. Bununla birlikte, aktif karbon katkılı GO fiber tarafından üretilen dokunmamış yapı, referans GO fiberinden yaklaşık 3 kat daha yüksek SO_2 adsorpsiyon kapasitesine sahiptir. Burada aktif karbon malzemesinin gözenekli yapısının da etkili olduğu diğer örneklerden daha yüksek gözenek çapı ve por hacmine sahip olmasından anlaşılabilir. Adsorpsiyon kapasitesi sonuçlarına uygun olarak, aktif karbon katkılı numune daha yüksek BET yüzey alanına sahiptir.

Hidrazin hidratla indirgenen numune ise FTIR analizinde görüleceği üzere, üzerinde uygun fonksiyonel grup bulunmaması nedeniyle en düşük adsorpsiyon kapasitesini göstermiştir. Tek koagülasyon banyosu ve PVA kaplanan numuneler ise yeni bağlantılar sağladığından referans numunelerden daha fazla kapasiteye sahiptir.

Bu çalışmanın ışığında, ileriki çalışmalar adsorpsiyon kapasitesini arttırmak üzere fonksiyonel grup eklenmesini sağlayabilecek yöntemler üzerine yapılabilir, bunun yanında aktif karbon gibi gözenekli yapılar veya nanopartiküller eklenerek adsorpsiyon kapasiteleri karşılaştırılabilir. Asidik bir gaz olan kükürt dioksit adsorpsiyonu için dispersiyonun pH değeri daha bazik olarak üretilebilir. Ayrıca diğer literatür araştırmalarındanelektrik iletkenliğini arttıracağı bilinen Vitamin C (Askorbik asit) ile indirgeme denenmesi çevre açısından daha uygun olacak, sonrasında zararlı bir artık kalmayacağından işlem süresini kısaltacaktır.

1. INTRODUCTION

Carbon plays a very important role in nature. The two-dimensional form of carbon is graphene, and the graphene was first mechanically obtained from graphite in 2004. It can be considered that the fullerenes and carbon nanotubes are formed by folding the graphene in spherical and cylindrical form, respectively. Grafen is distinctly different from carbon nanotubes and fullerenes and astonishes the world of science with its unique properties. Unlike carbon nanotubes, the graphene has a wider specific surface area, and the production cost of the graphene is lower than carbon nanotubes. This thinnest material obtained is the most resistant material in the world, its electrical and thermal conductivity is very high and elastic. Grafen has many application areas because of its ease of preparation and processing, as well as its wide range of manufacturability and low cost. The usage of graphene in the field of solar panels, energy storage, field effect transistors, sensors, and nanocomposites is promising. Also, it has usage areas as absorbance, catalyst, gas sensor etc.

The most common procedure used for graphene oxide is the oxidation of graphite particles. The oldest and most widely used process is known as the Hummers method. Graphene oxide has functional groups with oxygen-containing, negatively charged, hydrophilic structure.

Studies on the production of graphene oxide fibers by the wet spinning method have started to be published in scientific journals since the last month of 2011 and since they have a very recent past, literature is very limited about this research area.

The main purpose of this project is to produce graphene oxide fibers from graphene oxide and to examine sulfur dioxide adsorption capacity.

2. THEORETICAL BACKGROUND

2.1 Carbon

Carbon is the sixth element in the periodic table and has a molar mass of 12.011 $g.mol^{-1}$. It has two stable isotopes, namely they do not spontaneously change their structure and disintegrate, ^{12}C (98.9% of natural carbon) and ^{13}C (1.1% of natural carbon). It has a unique characteristic of being able to form bonds between its atoms creating stable compounds such as chains, branched chains, and rings. These molecular or crystalline forms are the allotropes (or polymorphs) of carbon, that is, they have the same building block (the element carbon) but with different atomic hybrid configurations: sp^3 (tetragonal), sp^2 (trigonal) or sp (diagonal) (Pierson, 1993; Morgan, 2005; Katsnelson, 2012).

2.1.1 The allotropes of carbon

Allotropes of carbon can be classified into three major categories: the sp^2 structures which include graphite, the graphitic materials, amorphous carbon, and other carbon materials, the sp^3 structures which include diamond and lonsdaleite (a form detected in meteorites), and the fullerenes (Pierson, 1993). The diamond and the graphite are three-dimensional, graphene is two-dimensional, the nanotubes are one-dimensional and the fullerenes are zero-dimensional allotropes of carbon (Katsnelson, 2007). Allotropes of carbon are given in Figure 2.1.

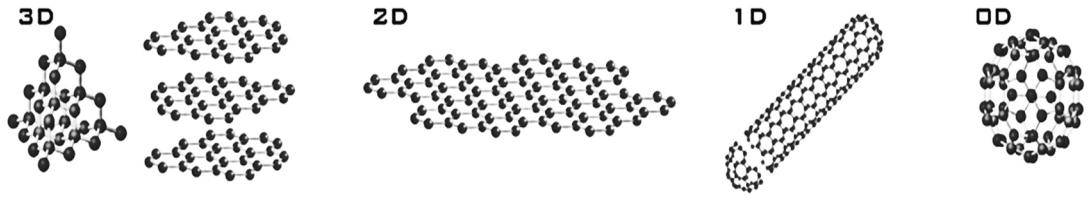

Figure 2.1 : Allotropes of carbon (Left to rigt), diamond and graphite (3D), graphene (2D), nanotubes (1D) and fullerenes (0D) (Katsnelson, 2007).

Diamond: Diamond has been known since the early history of mankind. It is hardest carbon form with a cubic structure which is thermodynamically stable at pressures above 6 GPa at room temperature and metastable at atmospheric pressure (Pierson,

1993, Morgan, 2005; Katsnelson, 2007). The diamond can be used to high temperatures and it starts to graphitize at about 1000°C in ambient air and at about 1400°C in vacuum. At low pressures and temperatures above 1900K in an inert atmosphere, diamond converts rapidly to graphite (Morgan, 2005; Fang, 2009; Mash and Reinoso, 2006).

Fullerenes: Fullerenes are another major allotrope of carbon which were discovered by British chemist Kroto and his team in 1985 and gained great attention in nanoscience field. They are symmetrically closed convex graphite shells, consisting of twelve pentagons and various numbers of hexagons. Fullerene molecules are in form of a hollow sphere, ellipsoid or tube (Morgan, 2005; Bakry et al, 2007).

Nanotubes: Carbon nanotubes (CNTs) are made by rolling up of sheet of graphene into a cylinder and they are most promising candidates in the field of nanoelectronics because of their unique electrical (CNT displays metallic, semiconducting and superconducting properties), chemical, mechanical (for example, the elastic modulus of SWNTs is much higher than steel that makes them highly resistant) and structural properties.Depending on the number of rolled-up graphene sheets, CNTs are divided into 3 general categories: single-walled (SWNT), double-walled (DWNT), and multiwalled CNTs (MWNT) as presented in Figure 2.2. (Malhotral et al, 2015; Kaushik and Majumder, 2015).

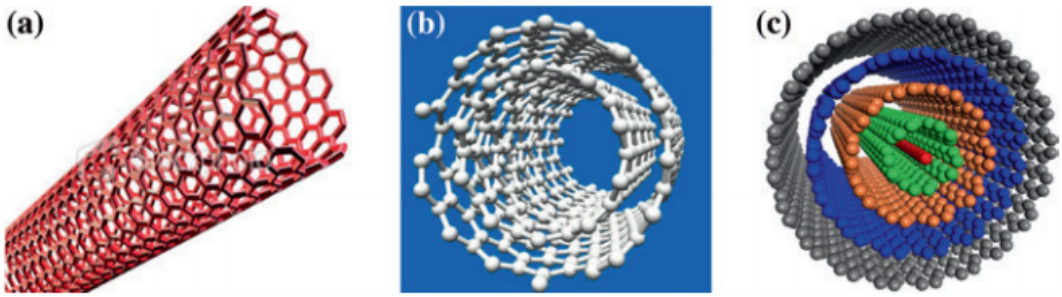

Figure 2.2 : Basic structures of a. SWNT, b. DWNT, and c. MWNT (Kaushik and Majumder, 2015).

Graphite: Graphite is a soft, opaque, conductor material and the most thermodynamically stable allotrope of carbon (Pierson, 1993; Fang, 2009).

Graphite is composed of series of stacked parallel layered material, consisting of a structure where carbon atoms are bound by covalent bonds to other carbons in the

same plane and only van der Waals forces are acting between successive layers (Pierson, 1993; Mukhopadhyay and Gupta, 2013; Uhl et al, 2005).

Graphene: Graphene is essentially a single carbon layer of graphite structure in the form of a hexagonal lattice of carbon atoms bonded in the sp^2 configuration. It was first isolated in 2004 by peeling off a layer of graphite on a piece of Scotch tape and in 2010, the Nobel Prize in Physics was awarded to Geim and Novoselov for their pioneering research on the structure and properties of graphene (Fang, 2009; Mukhopadhyay and Gupta, 2013).

As a new material, the uses of graphene are very attractive since many interesting properties which include unique chemical structure, superior electrical conductivity, high absorption of white light, high elasticity, unusual magnetic properties, high surface area, gas adsorption, and charge-transfer interactions with molecules (Rao and Sood, 2013; Sun et al, 2014).

2.2 Graphene Oxide

2.2.1 Structure

Graphene oxide (GO) is a two-dimensional (2D) material which is derived from the pristine graphene backbone by introducing several oxygen functionalities. Also, it can be considered as a monolayer of graphite oxide. By exfoliating graphite oxide into monolayered structures, GO sheets can be obtained.

In GO network, the oxygen atoms are covalently bonded to carbon atoms, converting them from the sp^2-hybridized state in the pristine graphene into the sp^3-hybridized state. In a typical graphene oxide structure, the number of carbon atoms bonded to oxygen exceeds the number of intact sp^2-hybridized carbon atoms. This makes GO very different from the parent graphene. On the other hand, these oxygen functionalities can be considered as defects which convert electrically conductive graphene into an insulator. However, the oxygen functionalities provide GO with many unique properties that the parent graphene does not have. One of these properties is hydrophilicity, i.e. the ability to be dissolved and to form stable colloid solutions in water and in some low-molecular-weight alcohols. Another advantage is opening a tunable bandgap that is responsible for unique optical and electronic

properties (Sattler, 2016; Zhao et al, 2015; Dimiev and Tour, 2014; Dimiev and Eigler, 2017).

Graphene oxide is comprised of hydroxyl, epoxide and carboxylic acid functional groups which are shown in Figure 2.3. (Muhamad et al, 2016).

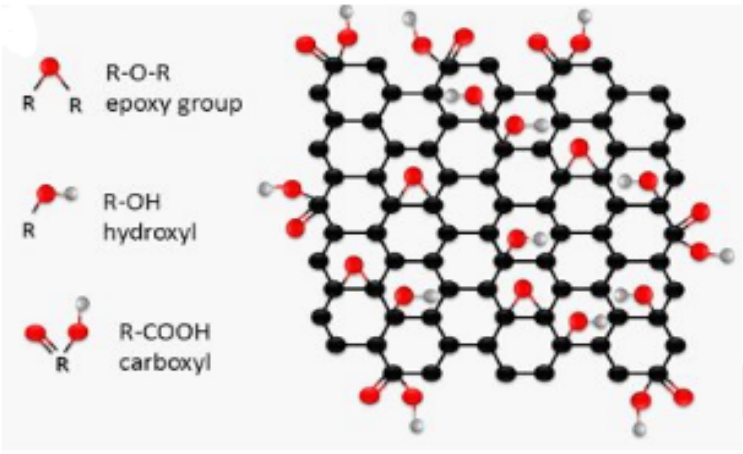

Figure 2.3 : Graphene oxide structure (Adapted from Chiu et al, 2013).

The hydroxyl and epoxide group are positioned at the basal plane, whereas the carboxylic acid group is placed at the edges (Muhamad et al, 2016).

2.2.2 Synthesis

Despite the relative newness of graphene as a material of broad interest and potential, GO has an older history than it (Dreyer et al, 2009). GO was firstly reported in 1840 by Schafhaeutl and 1859 by Brodie. Brodie first synthesized graphite oxide by adding potassium chlorate to the slurry of graphite in fuming nitric acid.

After about 40 years, Staudenmaier improved this method by replacing about two-thirds of fuming nitric acid (HNO_3) with concentrated sulfuric acid (H_2SO_4) and feeding the chlorate in batches.Based on these work, Hummers and Offeman developed an substitute oxidation method in 1958. This method is often called Hummers method, in which sodium nitrate ($NaNO_3$) and potassium permanganate ($KMnO_4$) dissolved in concentrated H_2SO_4 was used to oxidize graphite into graphite oxide within a few hours.

Thanks to the ease and short time of execution, Hummers' method was widely accepted, but there is still several flaws, including toxic gas generation (NO_2, N_2O_4), residual nitrate and low yield etc. To solve these problems, various modification on

Hummers' method have been proposed in the past 20 years (Pei and Cheng, 2012; Yu et al, 2016).

After synthesis of graphite oxide, GO can be obtained by exfoliating graphiteoxide into monolayer sheets through a variety of thermal and mechanical methods (Zhao et al, 2015) (Figure 2.4).

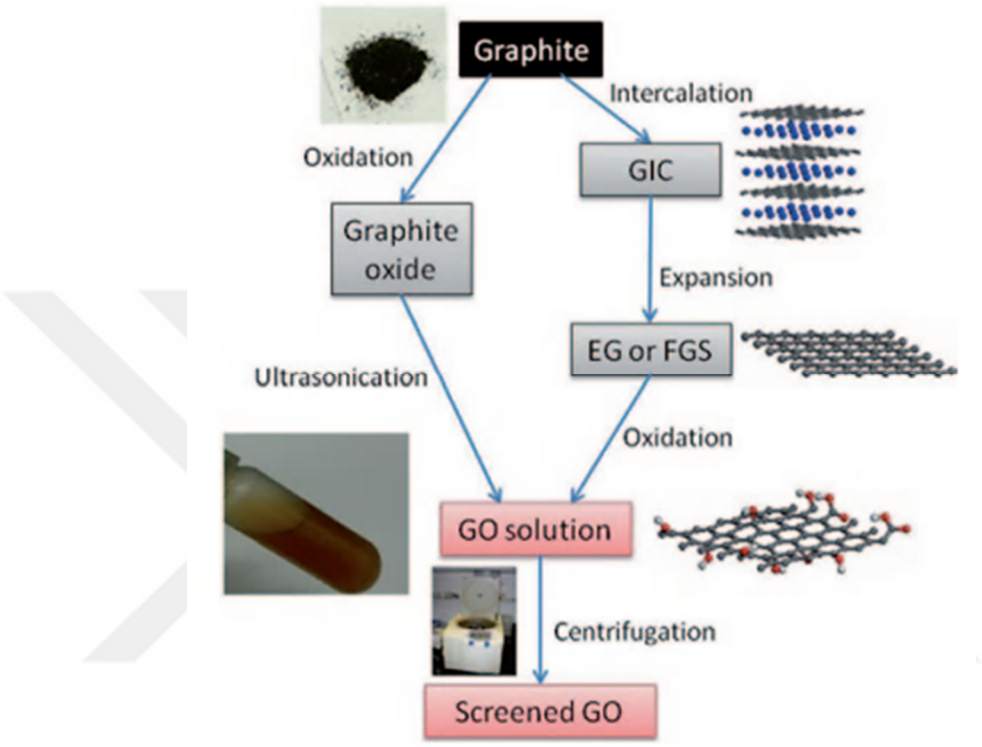

Figure 2.4 : The scheme for production of screened graphite oxide (GO) GIC graphite intercalation compound, EG expanded graphite, FGS functionalized graphite sheets (Zheng and Kim, 2015).

2.2.3 Applications

GO is a versatile material, which has attracted the interest of researchers in many branches of science and technology (Perrozzi et al, 2015).Thanks to the fact that GO has unique surface chemistry and architectures, such as three-dimensional network, extremely high surface area, tunable electrical conductivity, good chemical/electrochemical stability, high flexibility and excellent elasticity; it exhibits a moderate conductivity, high chemical stability, and excellent mechanical, optical, thermal, electrochemical properties. Hence, GO is deemed to be a desirable material in a broad range of applications such as gas sensors or storage, high-performance fibers, composite membranes, electrochemical applications, energy devices, field

effect transistors and so forth (Li et al, 2015; Chen et al, 2014; Muhamad et al, 2016).

Because of the large high surface area and abundant functional groups of GO, it is suitable as a component in energy storage devices. Also, it provides enough space and active sites for adsorption of gaseous molecules and various species in solutions, such as hydrogen storage, the capture of CO_2, CO, SO_2, NO_2, and NH_3gases for air purification, removal of heavy metal ions and organic containments for water purification (Muhamad et al, 2016; Li et al, 2015).

Because of its fluorescent properties, graphene oxide could be used in biosensing application. The tunable and controllable electronic properties of GO enable their promising applications in electronic devices (as a transparent conductive film) (Figure 2.5) and coating technology. For applications in lithium batteries and supercapacitors, the appropriate reduction can improve the electrical conductivity while keeping the inherent properties of GO (Muhamad et al, 2016; Li et al, 2015; Zhao et al, 2015).

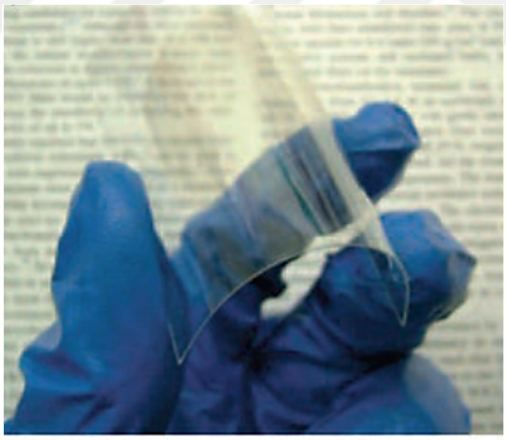

Figure 2.5 : Photograph of transparent GO thin film on plastic substrate (Sun et al, 2014; Eda et al, 2008).

Among carbon-rich materials, uncharacteristically, GO exhibits substantial cell membrane permeability and relatively low-level toxicity both in cellular assays and in vivo. In turn, it makes GO an interesting material for biomedical and medicinal applications. For instance, graphene oxide is used as a drug deliverer due to its ability in targeting tumor cell without affecting the normal cell. Also, owing to the excellent biocompatibility, ready cellular uptake, flexible chemical modifications and unique optical properties, GO has been explored for in vitro and in vivo imaging and

phototherapy.It could be applied as an antibacterial material by reason of its sharp edges which can penetrate the membrane wall and result in the inactivation of bacteria (Muhamad et al, 2016; Dimiev and Eigler, 2017; Yang et al, 2013).

The swelling of graphene oxide structure allows water to penetrate between individual graphene oxide layers. Because of the small pore of graphene oxide material, salt can easily be filtered hence it can be used for water purification (Muhamad et al, 2016).

Beside these, compositing with other materials, such as carbon materials, metals, metal oxides, conducting polymers and organic species will enable greatly improved performance and very broad application areas.

2.3 Sulfur Dioxide (SO_2) Adsorption on Graphene Oxide

Air pollution by industrial release of greenhouse and toxic gases into the atmosphere is one of the biggest threatens to the environment and human health (Li et al, 2015).The major air pollutant emitted in the combustion of fossil fuels including petroleum and coal, both major energy sources, is SO_2, a sulfur dioxide (Lee and Park, 2002). It is a colorless, malodorous and poisonous gas (İlhan, 2012). Except for anthropogenic effects, it is produced by natural ways like volcanoes and forest fires. It causes the greenhouse effect and photochemical smog (Chen et al, 2014), furthermore, can react with oxygen and water to form sulfuric acid that induces acid rains which threaten human health and nature severely(Manguna et al, 2001; Seredych et al, 2013; Shao et al, 2013).

One of the SO_2 removal way is adsorption which is used in this study. In previous studies, activated carbon (AC), activated carbon fibers (Ucar et al, 2016), metal oxides (Sasmaz and Wilcox, 2008; Dunn et al, 1999), porous adsorbents as zeolite (Marcu and Sandulescu, 2004; Yi et al, 2012), metal organic frameworks (MOFs) (Tan et al, 2013) and graphite-based materials (Seredych and Bandosz, 2010), (Chen et al, 2014; Shao et al, 2013; Seredych et al, 2013) were used as appropriate materials for SO_2 adsorption applications (Seredych and Bandosz, 2010). As a fiber form, because of its porous structure activated carbon fibers were generally studied (Manguna et al, 2001; Lee and Park, 2002;Ucar et al, 2016; Zhang et al, 2007; Tseng and Wey, 2004). As far as is known, there is not enough research about SO_2

adsorption capacity of GO fibers. Because of the functionalizable surface area of the material, porosity, the oxygen-containing functional groups on the basal plane which represent the adsorption sites, and chemical stability makes GO capable to covalently and noncovalently interact with various molecules (Perrozzi et al, 2015; Li et al, 2015) and acceptable adsorbent material (Manguna et al, 2001; Babu et al, 2016).

2.4 Wet Spinning Method

Among other spinning process (like dry, melt, gel spinning), wet spinning technique is the oldest and most complex method. In the process, a solution flow through a nozzle into a coagulation bath which is non-solvent for fiber. Fiber becomes rigid and orientation takes place thank to turning or pulling effect according to technique (Nakajima, 1994).

Figure 2.6 shows schematically the wet spinning process, where a solution is pumped into the syringe needle and the filaments thus produced in the spinning bath are passed through coagulation baths to yield solid filaments. The solvent originally added to the solution is removed in coagulation baths by the mechanism of counter-diffusion. Sometimes, a chemical reaction also takes place in the coagulation bath. This process is not economical as far as the melt spinning process because the removal of the solvent from the filaments is an additional cost. In general, more than one coagulation bath is used to remove the solvent, and sometimes the steps involved with after treatment (washing and drying) are used for further stretching the filaments.

In commercial wet spinning, a series of complex simultaneous operations are performed on and within each spun filament. These are extrusion in the spinneret hole, fiber elongation, molecular orientation, and coagulation.

Spinning under maximum tension, and therefore under maximum tensile stress, may improve the tensile properties of the finished fiber by increasing molecular orientation. Three factors that could affect spinnability and the mechanism of fiber breakage in the wet spinning process may be isolated: (1) coagulating bath concentration, (2) system temperature, (3) stretch ratio. Coagulating bath concentration is important because this factor actually determines the rate of coagulation, skin formation, take-up speed, maximum stretch ratio, and tensile

stress.Temperature is important primarily because it affects the shear viscosity of the spinning solution inside the spinneret hole and the elongational viscosity of the spinline under stretching. Its main influence on tensile stress and stretch ratio, rather than on coagulation rate. Strech ratio is listed independently because it is actually a measure of the filament residence time. Even under optimum conditions of temperature and coagulating bath concentration, the stretch ratio may be considered to be an independent variable (Han, 2007).

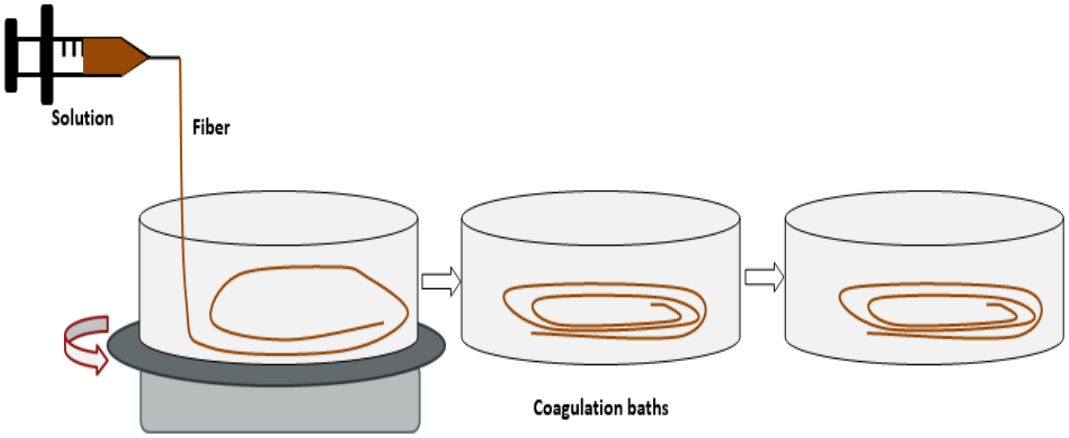

Figure 2.6 : Lab-scale production by wet spinning method.

3. EXPERIMENTAL PROCEDURE

3.1 Materials

Graphene-GIC (Grafen Co., expandable graphite, thickness 30 µm, diameter 300 µm, purity: 99%), $KMnO_4$ (Merck, M: 158.03 g/mol), H_2SO_4 (Merck, M: 98.08 g/mol), $NaNO_3$ (ZAG, 7631-99-4, M: 84.99 g/mol), HCl (Hydrochloric acid) (%37, Merck), Distilled water, Activated carbon nanoparticle (Grafen Co., average particle size (APS): <100 nm, purity: >%95), Hydrazine hydroxide (100%, Merck), Poly(vinyl alcohol) (ZAG, BP17), Hydrogen peroxide (30%, Merck), Sodium hydroxide (Merck), Phenol red indicator.

3.2 Thermal Exfoliation Process

The exfoliation of graphite is a process which increases surface area. It is intended that the next oxidation process is more efficient in this respect. A fixed bed tube furnace was used for the process (Figure 3.1).

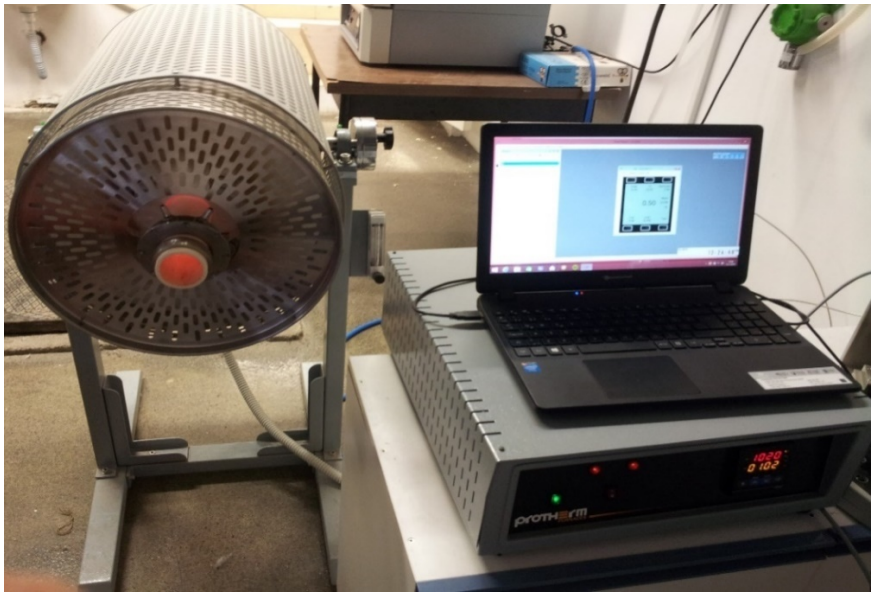

Figure 3.1 : Fixed bed tube furnace.

The exfoliation process was started in quartz tube which has two entrance for gas inlet and outlet. Dried expandable graphite was loaded into a quartz tube (0.4- 0.5 g).

Before loading the quartz tube to furnace, medium is purged with 0.5 SLPM (Standard Liter per Minute) argon for 10 minutes. Subsequently, the volumetric flow rate was set to 0.2 SLPM. The quartz tube was then quickly inserted into a furnace preheated to 1020 ºC, and within 35 seconds, exfoliation occurred (Figure 3.2).

Figure 3.2 : Exfoliation process.

3.3 Preparation of Graphite Oxide by Using Modified Hummer's Method

$KMnO_4$: H_2SO_4 = 1: 20 (w/w)

Graphite: H_2SO_4 = 1: 100 (w/w)

Graphite: $NaNO_3$ = 1: 0.5 (w/w)

Graphite oxide was produced based upon above ratios. In this method, 1 g of graphite and 0.5 g of $NaNO_3$ were mixed and 100 mL of sulfuric acid was added into solution kept under at a ice bath (0°C) with stirring continuously. After the acid was brought into contact with the sample thoroughly, 5 g of $KMnO_4$ was added slowly. The addition rate was controlled carefully to preserve the reaction temperature lower than 20°C, so the addition of potassium permanganate was done in 30-45 minutes. Stirring was carried out for 2 hours under ice bath. Then the ice bath was removed and the temperature was raised to 35°C and solution was stirred at this temperature for 2 hours. At the end of the mixing process, the mixture was diluted by slowly adding of 220 mL of distilled water in approximately 30-45 minutes in order to

avoid any chemical risk. Attention was paid to temperature control during addition. Additions were made carefully and slowly as sudden temperature increases may occur. Then, the temperature was increased to 98°C over 30 minutes and and the color changes to brown type of color and stirred at this temperature for 15 minutes. Terminally, 770 mL of water was stirred continuously to this solution mixture and the solution was kept waited for 5 days (Figure 3.3).

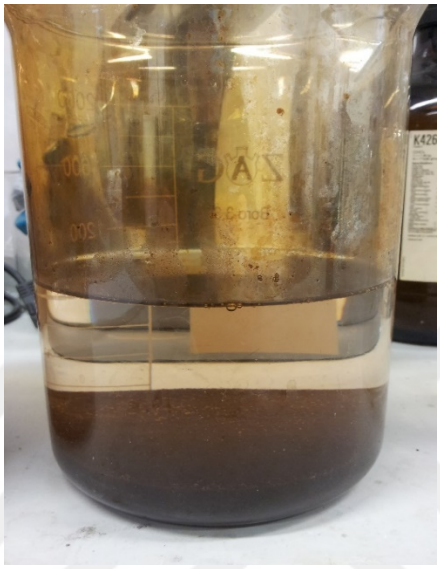

Figure 3.3 : The solution after 5 days.

The solution mixture was finally treated with 12 mL H_2O_2 for 15 minutes to terminate the reaction by the form of yellow colour (Figure 3.4).

Figure 3.4 : The solution after adding H_2O_2.

The day after, the upper aqueous part was decanted and separated. Graphite oxide was evenly distributed in the centrifuge containers. For purification, the mixture was washed by centrifugation (Nüve, NF800R) for 3 times with 1 M 500 mL HCl solution at 5500 rpm. Washing was then carried out with distilled water until pH-3 value is reached and the dispersion was seperated for pH-3 group fibers. Remaining dispersion were washed with distilled water until pH-5 value is reached for production of pH-5 group fibers.

3.4 Preparation of Graphene Oxide

Graphene oxide (GO) was produced from graphite oxide which produced with modified Hummers method through the instrument of mechanical homogenizer (WiseTis Homogenizer, HG-15D). For this treatment, the layers were dispersed for 90 minutes at 10000 rpm in a mechanical homogenizer.

3.5 Addition of Activated Carbon

Before activated carbon addition, the dispersion was adjusted to 20 mg / mL (20 mg graphene oxide per 1 mL water). Activated carbon was added as percentage of GO in the dispersion. After addition, mechanical homogenization was used to homogeneously disperse the nanoparticle in the dispersion. Produced fiber is called pH3 AC sample.

3.6 Fiber Production

The fibers were produced by the wet spinning method (at a feed rate of 20 mL/h) from graphene oxide dispersion by aid of laboratory syringe and passed through coagulation baths. Before this process, dispersion must be adjust to 20 mg / mL (20 mg graphene oxide per 1 mL water).

Adjusting GO dispersion to 20 mg / mL (20 mg graphene oxide per 1 mL water):

Petri dish (empty): x (gram)

Petri dish + graphene oxide sample: y (gram)

Petri dish + graphene oxide sample after dehydration at 47^{o}C in oven: z (gram)

Solid quantity: (z-x) g = (z-x).1000 mg

Water quantity: (y-z) g = (y-z) mL

mg/mL = [(z-x).1000] / (y-z)

Following that calculations, fiber production was done with syringe pump mechanism which is shown in Figure 3.5.

Figure 3.5 : The mechanism which is used for fiber production by wet spinning method.

The GO dispersion was injected into the A, B, and C type coagulation baths (Figure 3.6) respectively at a feed rate of 20 mL/h, through needle with 0.69 mm inner diameter (thickness: 19 gauge).

The contents of the coagulation baths are as follows:

Bath A: 30 mL/70 mL (ethanol/water) + 5 % wt $CaCl_2$ (5 gram)

Bath B: 40 mL/60 mL (ethanol/water)

Bath C: 50 mL/50 mL (ethanol/water)

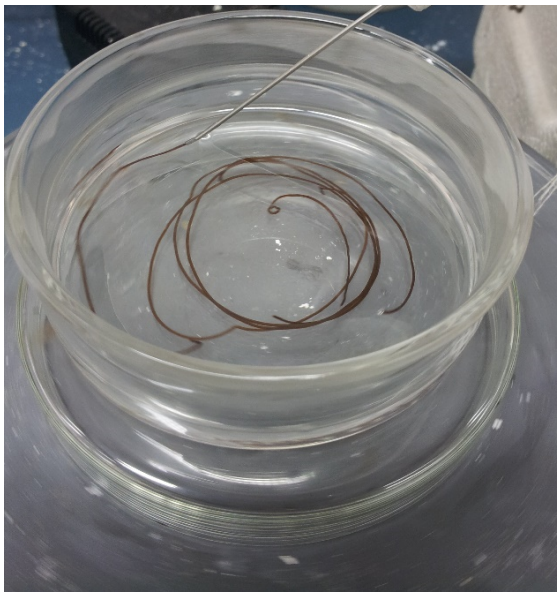

Figure 3.6 : Fibers in coagulation bath.

The obtained fibers were dried in room conditions and made prepared for testing.

3.7 Reduction of GO Fibers

Reduction of GO fibers was carried out by two methods; reduction by hydrazine (hydrazine hydroxide) vapor and reduction by immersing to hydrazine.

Reduction by hydrazine vapor: GO fibers were placed in a perfectly cleaned glass Petri dish inside a larger glass Petri dish which contained 1 mL of hydrazine hydroxide 100% (hydrazine hydrate). But, the amount of the substance was insufficient, the reduction could not take place, and 5 mL of 100% hydrazine hydroxide was put on it and the reduction was successful in this amount. Then, the larger dish was covered with a glass lid, sealed with aluminum foil, and placed on a hot plate at 80 °C for 3 h. Better results were obtained by increasing the amount of hydrazine. The presence of more hydrazine in the medium allows more hydrazine vapor to interact with the fiber by providing more hydrazine vapor. GO fibers changed color after the hydrazine vapor treatment, from black to dark black, indicating the reduction of the material (Figure 3.7). But, according to FTIR results, this method did not provide enough reduction and the fibers were reduced by another method.

a. 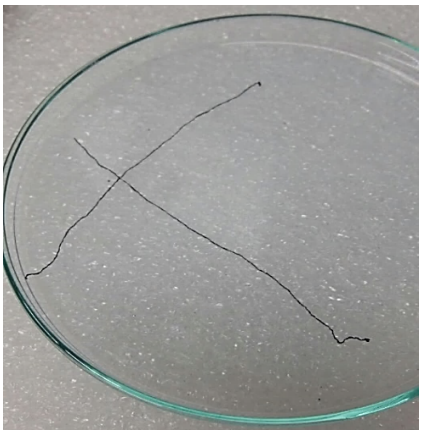 b. 

Figure 3.7 : Reduction by hydrazine vapor a. non-reduced GO fiber, b. reduced GO fiber by hydrazine vapor.

Reduction by immersing into hydrazine: Additionally, we tried to reduce our GO samples by immersing into hydrazine.. For this process, the GO fibers were immersed into the 5 mL of hydrazine hydroxide solution and kept for 20 minutes. Then, fibers were dried at 80ºC for 2 hours to get rid of excess hydrazine before characterization (Figure 3.8). Produced fiber is called pH3 hydrazine sample.

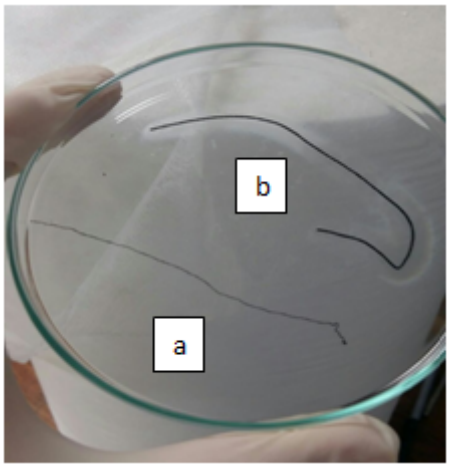

Figure 3.8 : Reduction by immersing into hydrazine hydrate a. non-reduced GO fiber, b. reduced GO fiber.

3.8 GO Fiber Production by Single Coagulation Bath

Differently from regular production, here, only one bath was used. This bath was contained 100 mL ethanol and 5 % wt $CaCl_2$ (no water). Fibers were synthesized in this bath and then they were dried at room conditions.Produced fiber is called pH3 single coagulation sample.

3.9 Poly (vinyl alcohol) (PVA) coated fiber production

For the pH5 PVA coated samples, only the Bath C was changed. The contents of the coagulation baths are as follows:

Bath A: 30 mL/70 mL (ethanol/water) + 5 % wt $CaCl_2$ (5 gram)

Bath B: 40 mL/60 mL (ethanol/water)

Bath C: 50 mL/50 mL (ethanol/water) + PVA (10 % of water) (5 gram)

Produced fiber is called pH5 PVA sample.

3.10 Characterization

3.10.1 Scanning electron microscopy (SEM)

Analyses of morphological surface of fibers were performed by a Quanta FEG 250 (15 kV) scanning electron microscope (mag: 1000x, 1200x and 20000x).

3.10.2 Tex number

The Tex number is the mass in grams of 1000 m of the yarn.Three of the sample fibers are selected and their length measured. The weights of the fibers are determined with the help of the precision scale. After determining the total length of the fibers and the total weight, the weight to be obtained for the fiber of 1 km length is found.

3.10.3 X-ray diffraction (XRD)

X-ray diffraction analysis was done to know the crystal size and crystal phase and structure of the synthesized samples. X-ray diffraction patterns were performed using a powder XRD system (PW3040) with CuK α radiation ($\lambda = 0.154$ nm).

3.10.4 Conductivity

The resistance of the fiber samples in 1 cm length were measured with a two probe Microtest 6370 LCR meter. The electrical conductivity is calculated by Equation 3.1.

$$\rho=(A*R)/L \qquad (3.1)$$

where; ρ= coefficient of electrical conductivity (S/cm), R= electrical resistance (ohm), A= cross sectional area of fiber (cm^2) and L= Fiber length between the probes (cm). Average value of 15 measurements has been taken.

3.10.5 Atomic force microscopy (AFM)

Atomic force microscopy (Ambios Technology, Santa Cruz, CA) was carried out in tapping mode under ambient conditions by using a silicon nitride tip with a radius of less than 8 nm.

3.10.6 Fourier transform infrared spectroscopy (FTIR-ATR)

FTIR-ATR spectra were recorded by using Perkin Elmer FT-IR C99089 in spectral range from 400-4000 cm^{-1}.

3.10.7 Raman spectroscopy

Raman spectra were recorded with Renishaw Invia spectrometer using the exciting line at 532 nm of a laser (10% power, 3-6 mW) for 20 second. Laser beam was focused with a 50x objective.

3.10.8 Thermogravimetric analysis (TGA)

TGA was further used to characterize the thermal properties ofthe nanocomposites. Thermogravimetric analysis (TGA) was carried out on a TA SDT Q600 instrument in the temperature range of 0–350 ^oC in a N_2 atmosphere, at a heating rate of 10 ^oC min^{-1}.

3.10.9 Brunauer-Emmett-Teller (BET) surface area analysis

Calculation of the surface area was carried out by Brunauer-Emmett-Teller (BET) method by using Quantachrome Quadrosorb SI and nitrogen gas. Degassing of samples were done for 24 hours at 75 °C before measuring the surface area and pore information.

4. EXPERIMENTAL RESULTS

4.1 Scanning Electron Microscopy (SEM)

The morphology of GO fibers is given between Figure 4.1 and Figure 4.6.

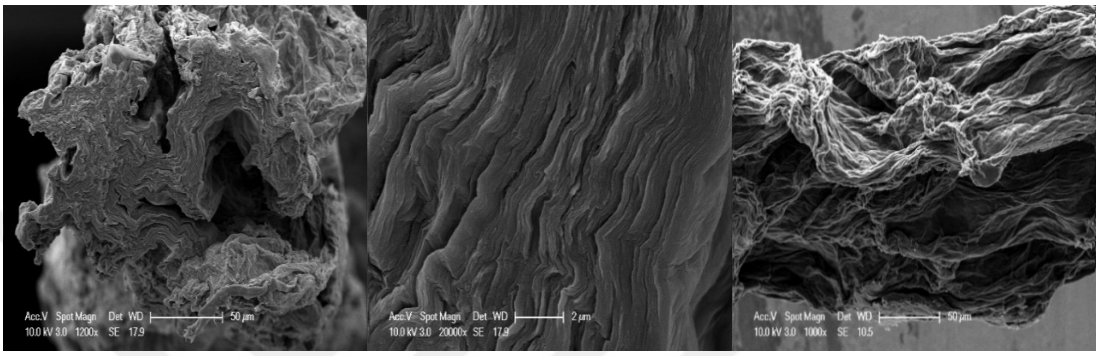

Figure 4.1 : SEM micrographs of pH3 reference sample, cross sectional (1200x), cross sectional (20000x) and longitudinal appearance (1000x), respectively.

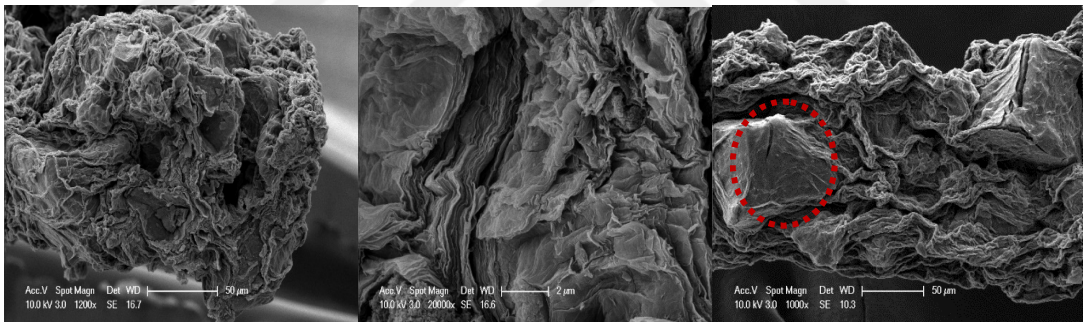

Figure 4.2 : SEM micrographs of pH3 AC sample, cross sectional (1200x), cross sectional (20000x) and longitudinal appearance (1000x), respectively.

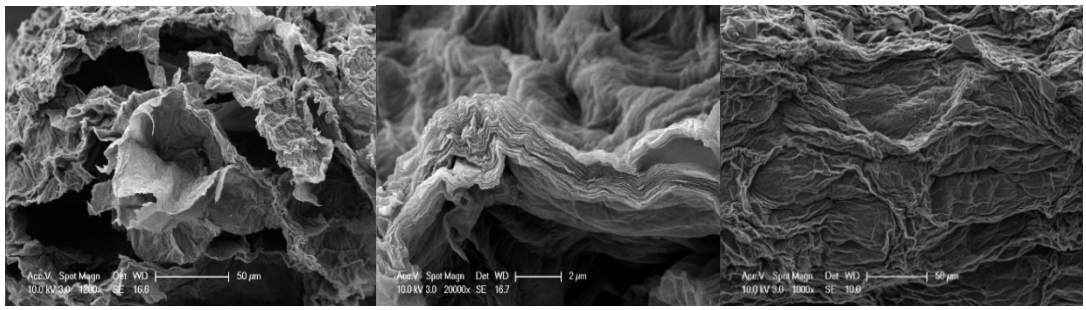

Figure 4.3 : SEM micrographs of pH3 hydrazine sample, cross sectional (1200x), cross sectional (20000x) and longitudinal appearance (1000x), respectively.

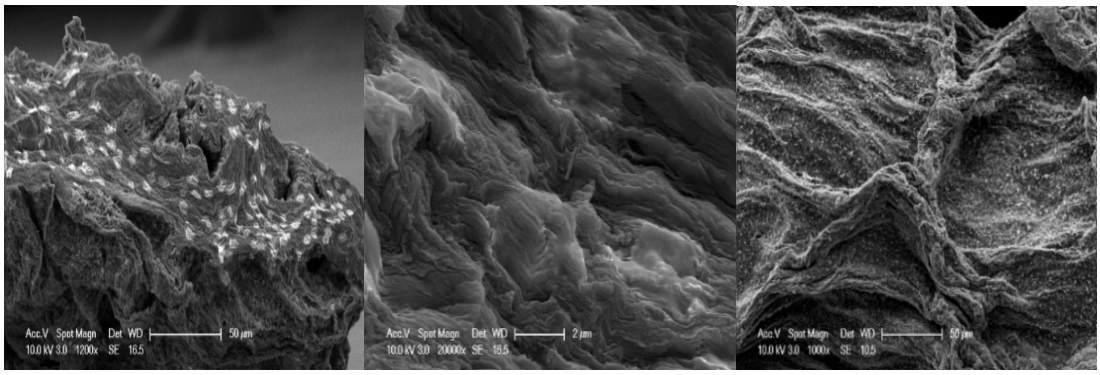

Figure 4.4 : SEM micrographs of pH3 single coagulation sample, cross sectional (1200x), cross sectional (20000x) and longitudinal appearance (1000x), respectively.

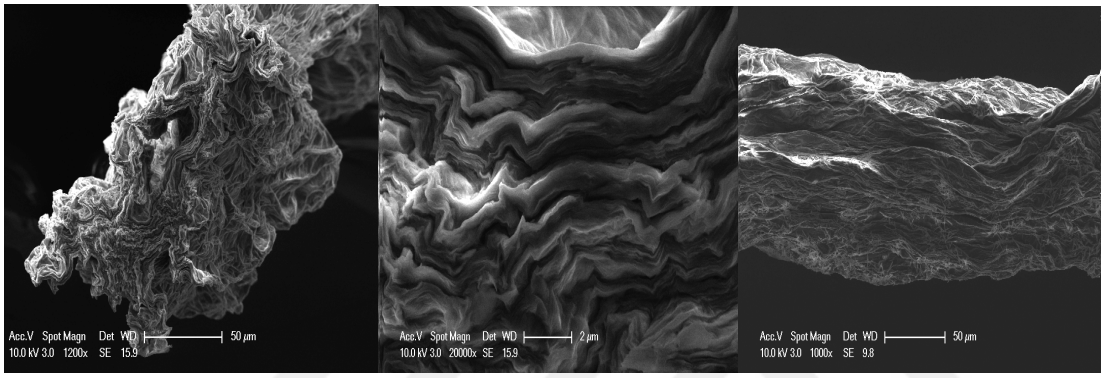

Figure 4.5 : SEM micrographs of pH5 reference sample, cross sectional (1200x), cross sectional (20000x) and longitudinal appearance (1000x), respectively.

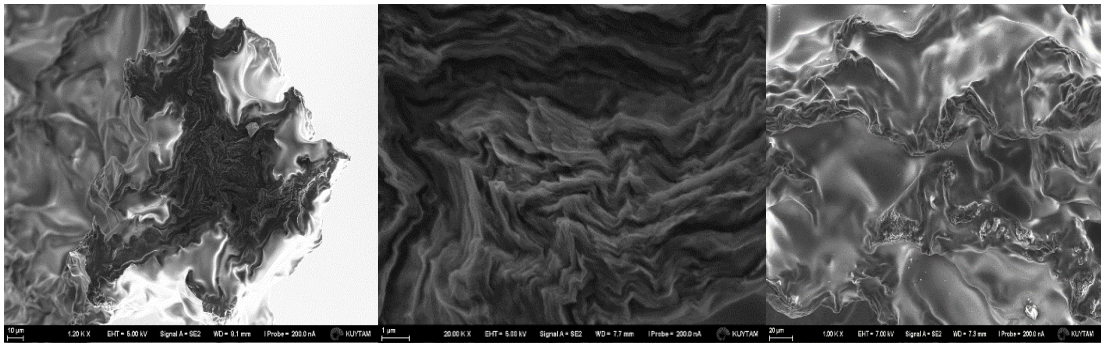

Figure 4.6 : SEM micrographs of pH5 PVA sample, cross sectional (1200x), cross sectional (20000x) and longitudinal appearance (1000x), respectively.

As can be seen from Figure 4.1 and Figure 4.5, layers were uniformly visible for pH3 and pH5 reference samples, while layers of AC-doped fibers were distorted (Figure 4.2). Marked area with red shows activated carbon nanoparticle. It can be said that the difficulty of fiber drawing originated here.

It has been observed that the layered smooth fiber structure degraded by hydrazine dipping (Figure 4.3). On the single coagulation fiber, the crystal structures are

covered the entire fiber, and crystal structures were observed in the zoomed image (Figure 4.4).

In Figure 4.6, the places on the fiber that are visible in gel form belong to PVA. In cross-sectional appearances, it is seen that PVA fill the voids by entering into the fiber.

4.2 Tex Number

Tex number values of GO fibers are shown in Table 4.1.Between pH3 reference, pH5 reference, and pH3 hydrazine samples, there is no significant change in Tex values. On the other hand, the Tex value increased by the addition of active carbon and PVA.During the single coagulation process, the structure became extremely curved and crimped fibers were synthesized (Figure 4.7). Because of this crimped structure, mass per unit length was increased, herewith Tex value of single coagulation sample was calculated the maximum value.

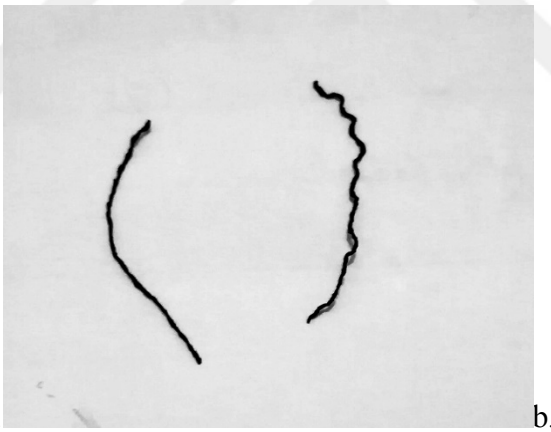

a. b.

Figure 4.7 : a. pH3 reference fiber b. pH3 single coagulation fiber.

Table 4.1 : Tex values of GO fibers.

Sample	Tex
pH3 Reference	13.92
pH3 AC	18.18
pH3 Hydrazine	14.29
pH3 Single coagulation	57.01
pH5 Reference	12.0
pH 5 PVA	20.05

4.3 X-ray Diffraction (XRD)

Table 4.2 represents the XRD results of fibers.Graphite (GIC) and thermally exfoliated graphite showed a characteristic peak at 2θ = 26.5º(Figure 4.8, Figure 4.9) and the distance between layers was 3,37 Å (Blanton ve Majumdar, 2012).As mentioned in the studies of Valapa et al(2015) and Saner et al, (2010), the number of layers and crystalline size increased in the wake of exfoliation at high temperature.

Table 4.2 : XRD analysis of GO fibers.

Sample	% Crystalinity	Crystalline size (Å)	d_{hkl}	Number of layers
Graphite (GIC)	91,1	117	3,37	35
Thermally exfoliated graphite (1020ºC-35 sec.)	86,7	686	3,32	206
pH3 Reference, Fiber (GO peak)	73.4	30	8.49	4
pH3 Reference, Dispersion (GO peak)	93.3	60	8.05	7
pH3 AC,Fiber (GO peak)	66.1	40	8.12	5
pH3 AC, Fiber (AC peak)	66.1	604	3.32	182
pH3 AC, Dispersion (GO peak)	68	49	7.61	6
pH3 AC, Dispersion (AC peak)	68	484	3.31	146
pH 3 Hydrazine, Fiber (Graphitepeak)	49.5	1194	3.34	357
pH 3 Single coagulation,Fiber (GO peak)	90.2	355	7.56	50
pH 3 Single coagulation,Fiber ($CaCl_2$peak) (2 teta:25.6º)	90.2	470	3.47	135
pH 3 Single coagulation, Lif ($Ca(OH)_2$ peak) (2 teta: 20.8º)	90.2	468	4.26	110
pH 5 Reference, Fiber (GO peak)	40.9	38	7.52	5
pH 5 Reference,Dispersion (GO peak)	95.2	86	7.94	11

After the introduction of oxygen functionalities for graphene oxide (GO), the graphitic peak shifted to about 2θ = 10º(Figure 4.10, Figure 4.11) and interlayer

distance between sheets was in the range of 7-9 Å (Cong et al, 2012). When activated carbon (AC) was added, new peak around 2θ=26° appeared (Figure 4.12, Figure 4.13) and interlayer distance was around 3 Å (Yusof et al, 2016; Singh et al, 2010).

With reduction by hydrazine hydrate, oxygenated groups were removed, the GO peak disappeared and graphitic peak observed at 2θ=26° (Figure 4.14).The interlayer distance was measured 3.34 Å because the epoxy and hydroxy groups are removed by reduction. In this way, it can be said that sample shows properties of graphite (Park et al, 2012). Due to the chemical reduction, large crystals have begun to be formed again on the graphene plane (Chen and Yan, 2011).

In pH5 sample (Figure 4.16, Figure 4.17), lower interlayer distance and higher crystal size were observed than in pH3 samples. This is because the solution is more stable at pH5 [Konkena and Vasudevan 2012; Kashyap et al, 2014) It is considered that there are stronger bonds in this stable dispersion which cause closer sheets and larger crystal structures between layers.

It was observed that the increase in the number of layers and a large crystal packing is present in the fibers produced by the activated carbon addition. The high and sharp peaks indicate that the crystal size is high (Monshi et al, 2012).

For single coagulation bath sample (Figure 4.15), there wasn't additional washing bath, so different groups have emerged. Since $CaCl_2$ can be separated into its ions (Ca^{2+} and Cl^-) in ethanol (Kohno et al. 2000), it is thought that these ions formed $Ca(OH)_2$ together with ethanol.However, it can be some non-ionizing $CaCl_2$ forms or they can be present only as ions.In the literature, XRD peaks of calcium hydroxide have been given at 2θ =18° and 2θ =34° (Kishar et al., 2013; XRD Pattern, 2017)

The peak at 2θ =24,5° has been referred to $CaCl_2$ (Nirmala et al., 2011). Based on this, it can be said that the peak of 2θ =25-26° degrees belongs to $CaCl_2$. When we look at the XRD patterns of the aqueous form of $CaCl_2$, it can be said that also the peaks between 2θ =15° and 21° and 2θ =29° to 34° degrees belong to this (Uriarte et al, 2015, Swanson et al, 1974).

When the dispersion and fiber samples are compared, the crystal size and crystallinity grade in the dispersion samples are generally slightly higher than fiber

and the interlayer distance value is slightly lower and therefore the number of layers is slightly higher. Here, it is thought that crystal structures are broken into small pieces by high shear forces when they are turned into fibers.

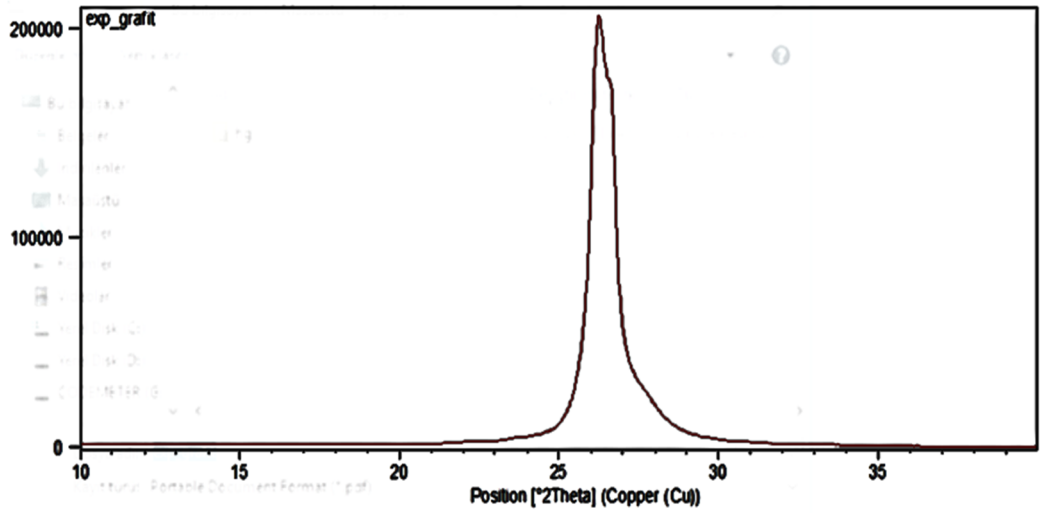

Figure 4.8 : XRD pattern of graphite (GIC).

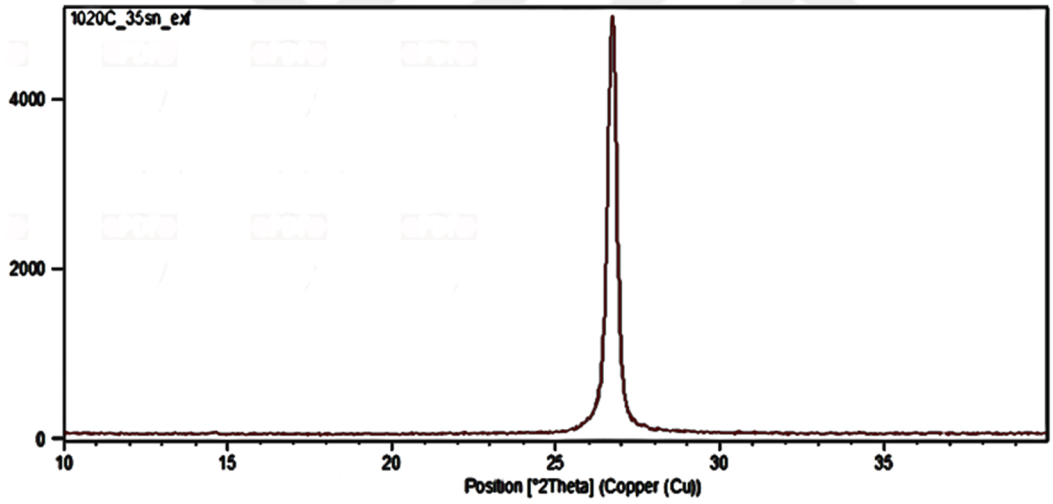

Figure 4.9 : XRD pattern of thermally exfoliated graphite (1020ºC-35 sec.).

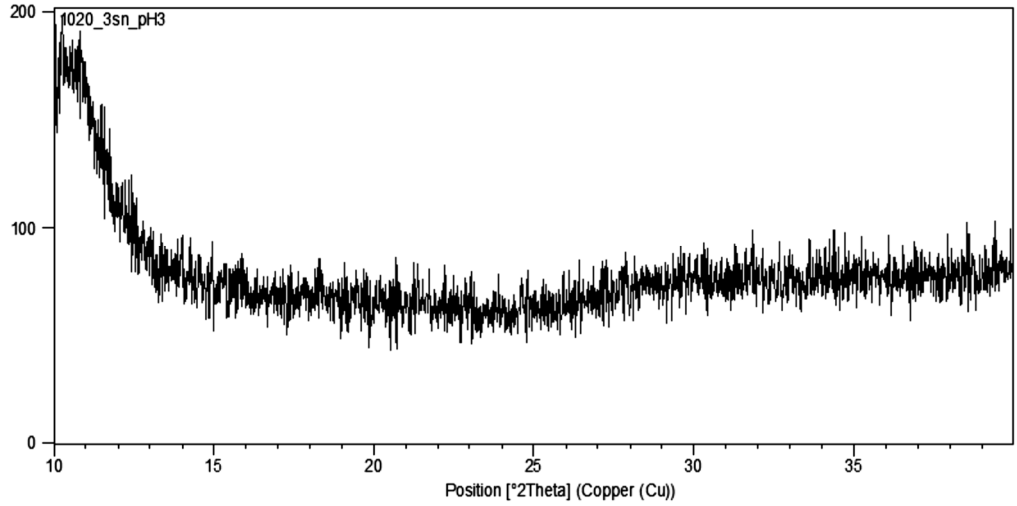

Figure 4.10 : XRD pattern of pH3 Reference fiber.

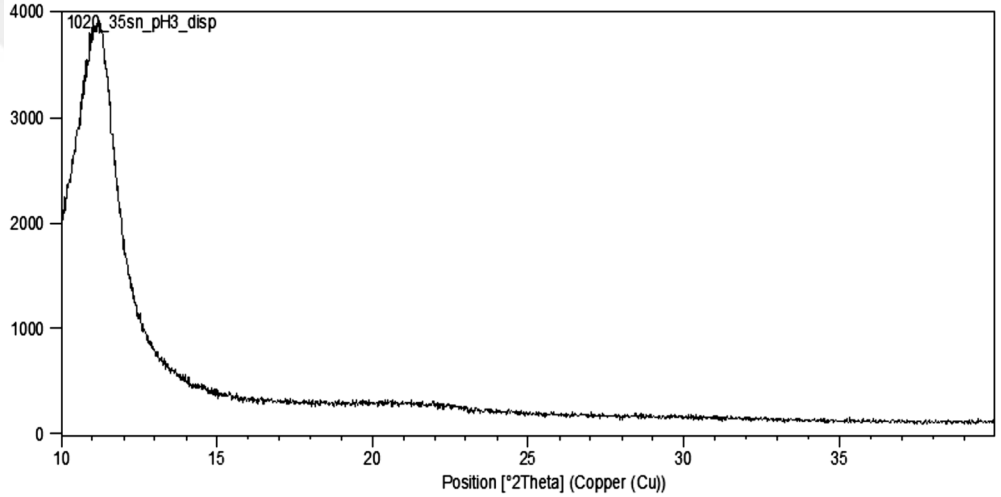

Figure 4.11 : XRD pattern of pH3 Reference dispersion.

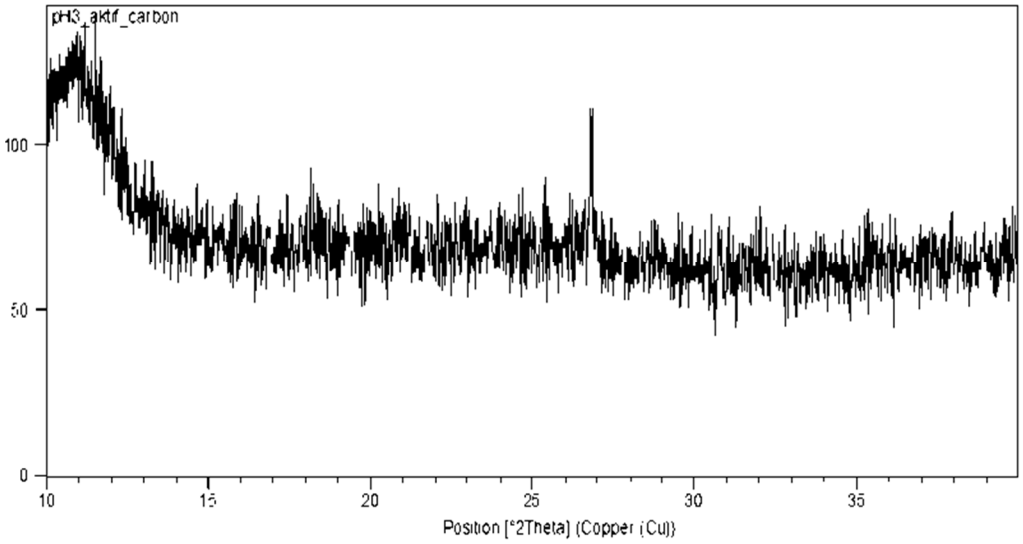

Figure 4.12 : XRD pattern of pH3 AC fiber.

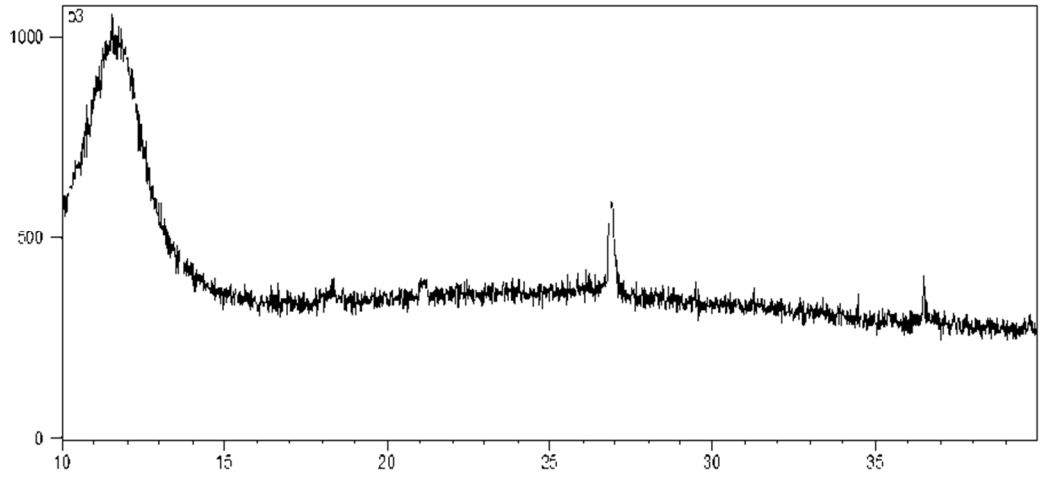

Figure 4.13 : XRD pattern of pH3 AC dispersion.

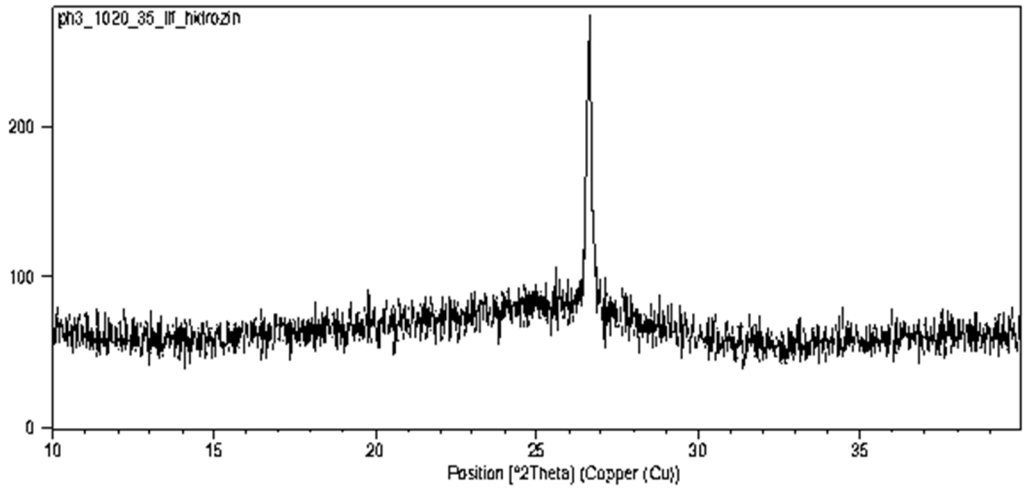

Figure 4.14 : XRD pattern of pH3 Hydrazine fiber.

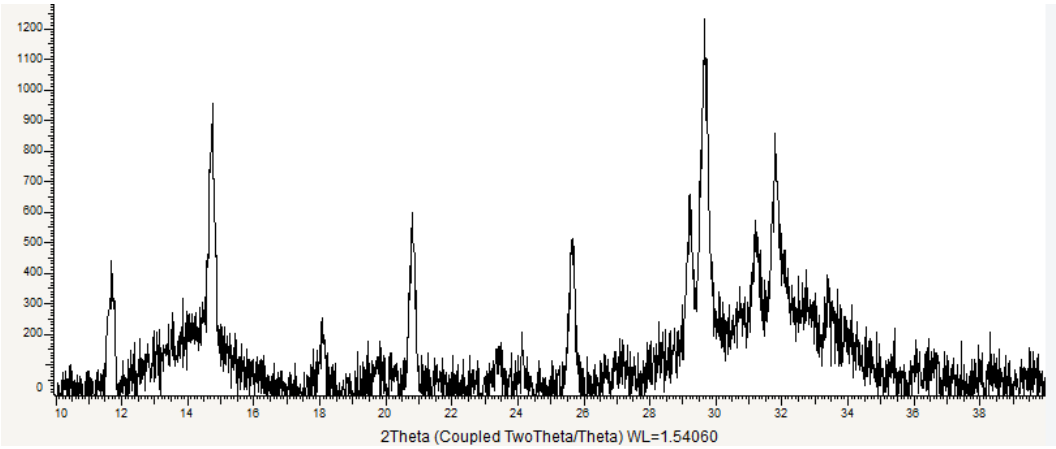

Figure 4.15 : XRD pattern of pH3 Single coagulation fiber.

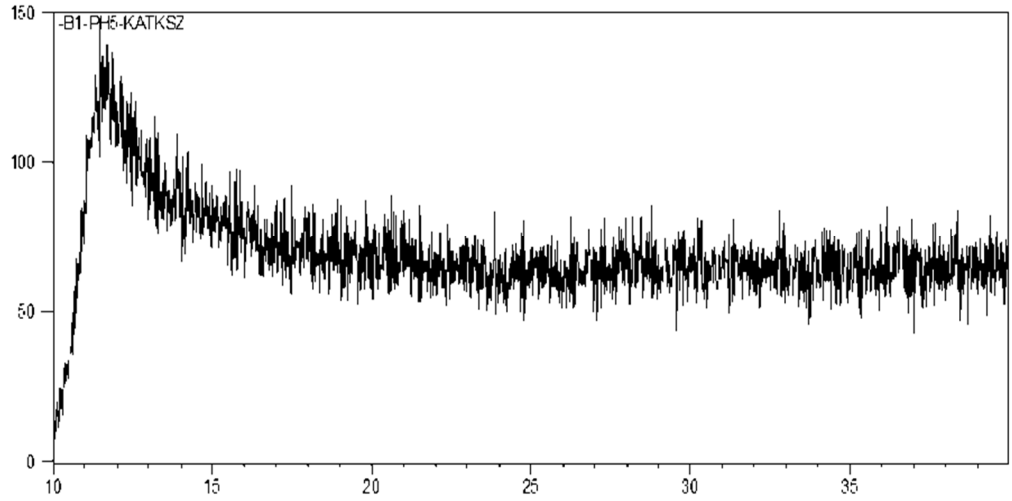

Figure 4.16 : XRD pattern of pH5 Reference fiber.

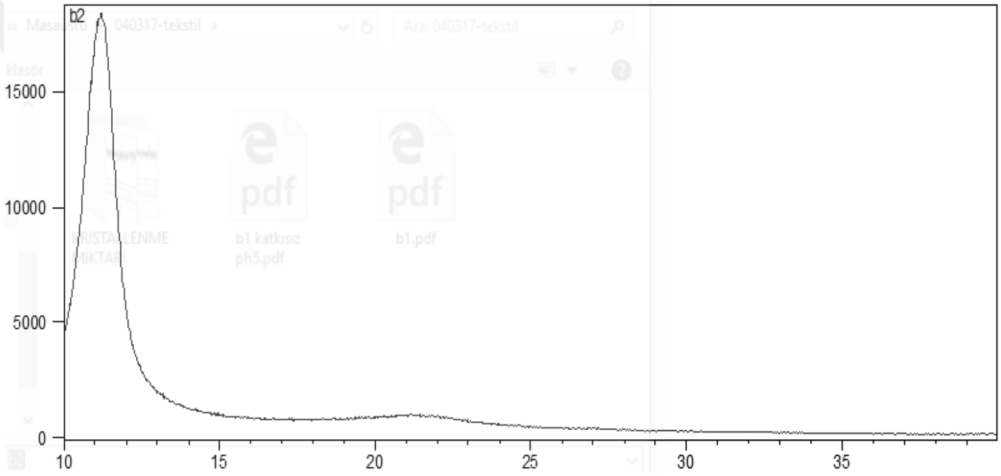

Figure 4.17 : XRD pattern of pH5 Reference dispersion.

4.4 Conductivity Results

Table 4.3 shows electrical conductivity of fibers. Here, pH3 single coagulation sample showed highest electrical conductivity.Because of fragile structure of pH3 hydrazine sample conductivity could not be measured (Table 4.3).

It seems that the conductivity of pH5 reference was slightly higher than pH3 reference, which may be due to the fact that the pH5 fiber has a more compact, more homogeneous and unfolded structure. Single coagulation sample had the highest electrical conductivity. It is known that $CaCl_2$ improves the electrical conductivity (Electrical Conductivity of Aqueous Solutions, 2017). No increasing effect of PVA addition was seen on electrical conductivity.

Table 4.3 : Electrical conductivity of GO fibers.

Sample	Average Conductivity (S/cm)	Standard deviation	Coefficient of variation (CV%)
pH3 Reference	$5.03*10^{-4}$	$6.4*10^{-4}$	12.7
pH3 AC	$5.51*10^{-4}$	$7.02*10^{-5}$	12.7
pH3 Single coagulation	$1.3*10^{-2}$	$3.02*10^{-3}$	23.3
pH5 Reference	$2.35*10^{-3}$	$4.94*10^{-4}$	21
pH5 PVA	$2.93*10^{-4}$	$8.28*10^{-5}$	28.3

4.5 Atomic Force Microscopy (AFM)

The obtained results from AFM analysis are given in Table 4.4.

Table 4.4 : Information of the surface morphologies of GO fibers.

Sample	Rq(μm)	Ra (μm)	Rpv (μm)	Rz (μm)
pH3 Reference	0.538	0.440	3.095	2.969
pH3 AC	0.366	0.276	2.572	2.407
pH3 Hydrazine	0.694	0.567	3.675	3.666
pH3 Single coagulation	2.875	0.546	0.427	2.850
pH5 Reference	0.829	0.642	4.963	4.948

pH5 reference sample was rougher than pH3 reference and pH3 AC sample (Figure 4.18, Figure 4.19, Figure 4.22).Hydrazine-reduced fiber increased the roughness due to voids and defects in the structure (Figure 4.20). In the case of single coagulation (Figure 4.21), the roughness increases the roughness according to Ra, which is considered to be more sensitive. As shown in the SEM image (Figure 4.4), the $CaCl_2$ salts on the fiber caused this sudden change due to sudden coagulation, which may cause the roughness to increase.

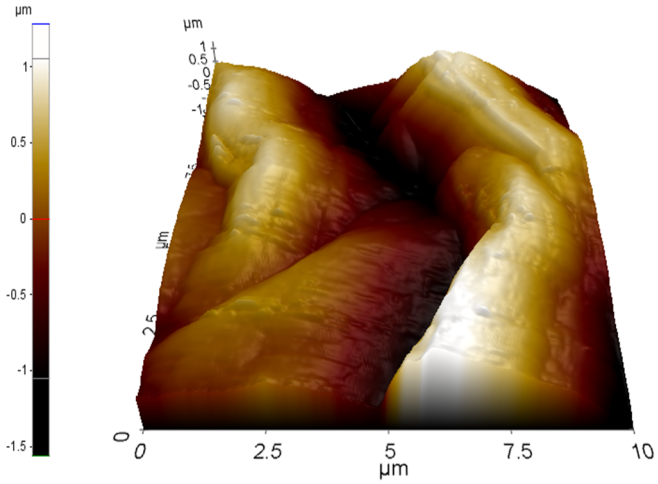

Figure 4.18 : AFM image of pH3 Reference.

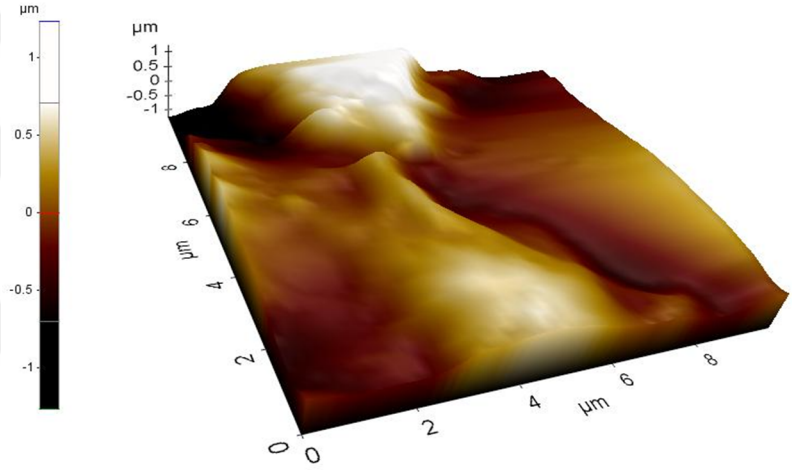

Figure 4.19 : AFM image of pH3 AC.

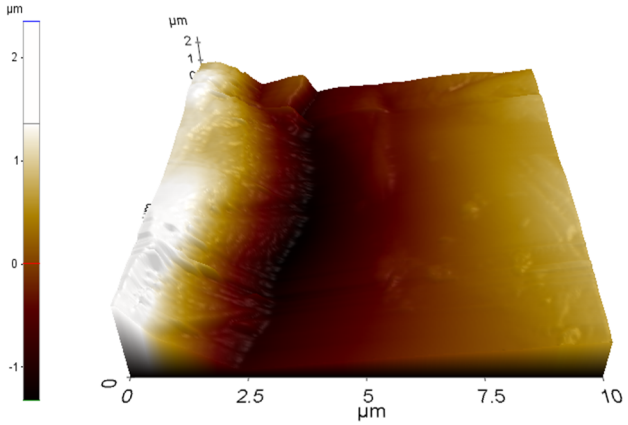

Figure 4.20 : AFM image of pH3 hydrazine.

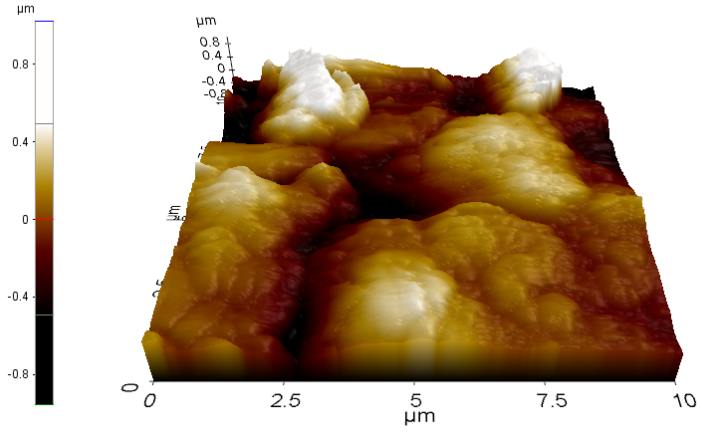

Figure 4.21 : AFM image of pH3 Single coagulation.

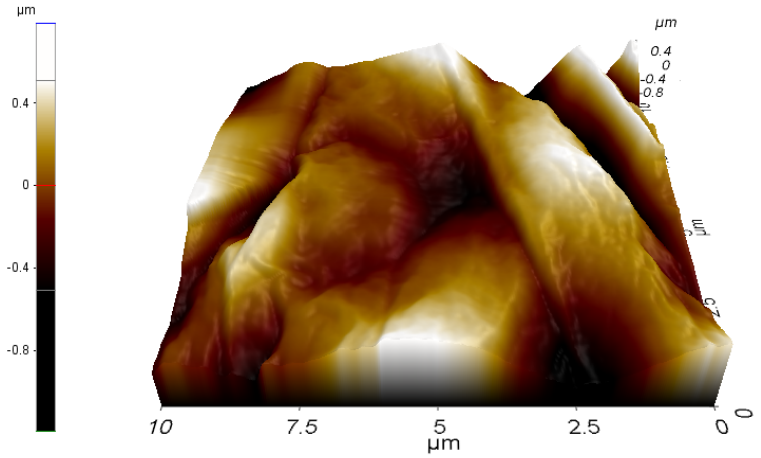

Figure 4.22 : AFM image of pH5 Reference.

4.6 Fourier Transform Infrared Spectroscopy (FTIR)

The same peaks were observed in the FTIR spectra of pH3 and pH5 reference fibers (Figure 4.23). Here, the broad peak between 3000- 3700 cm^{-1} belongs to the O-H bond stretching in the hydroxyl group, the peaks at 2982 cm^{-1} and 2881 cm^{-1} belong to the stretching vibrations of symmetric and antisymmetric CH_2, respectively. The weak peak at 1700 cm -1 belongs to the C = O bond stretching of the carbonyl and carboxyl groups. The peaks at 1590 cm^{-1}, 1366 cm^{-1}, and 1039 cm^{-1} belong to C=C bonds of aromatic structures, C-OH stretching bonds and C-OC stretching bonds of epoxy groups, respectively. Very small vibrations at 978 cm^{-1} refer to another epoxy, ether and peroxide groups in the structure (Kumar et al, 2017; Loryuenyong et al, 2013; Fernandez-Merino et al, 2010).

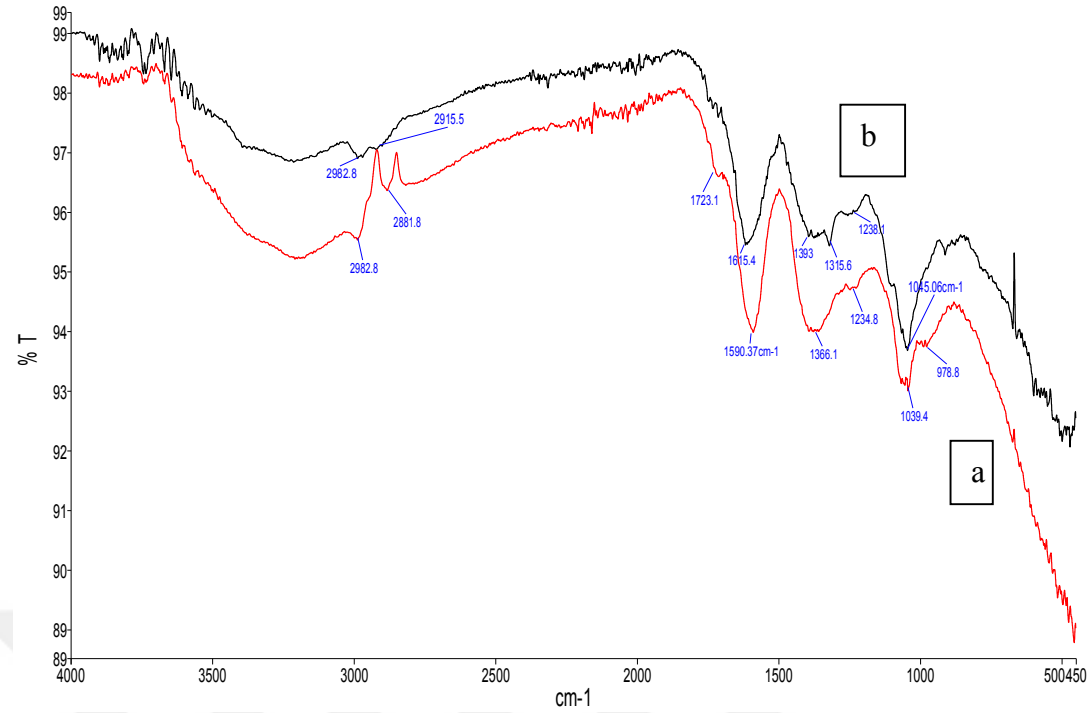

Figure 4.23 : FTIR spectra of a. pH3 reference ve b. pH5 reference.

Differently from the reference fibers; in spectra of AC doped sample (Figure 4.24), an increase in peaks from 1000 cm^{-1} to 1300 cm^{-1} was observed, these peaks belong to the C-H bond stretching and bending of the sample structure. In addition, due to the lack of O-H bonds, a broad peak reduction of 3000-3500 cm^{-1} was observed. These bonds are thought to be reformed by activated carbon bonds.

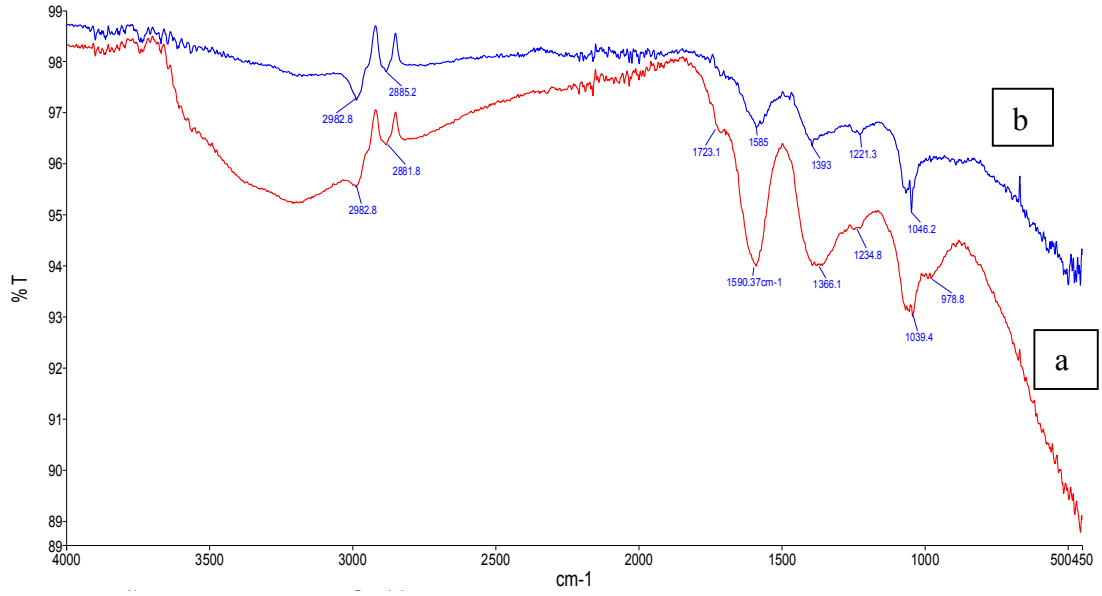

Figure 4.24 : FTIR spectra of a. pH3 reference ve b. pH3 AC.

For reduced sample, the disappearance of oxygenated functional groups is consistent with the disappearance of the most of the peaks (Figure 4.25).The large peak at 3000-3500 cm^{-1} which indicate O-H bond was disappeared. The peak at 1554 cm^{-1} belongs to the C = C bond and the shift was observed due to the absence of oxygen-containing functional groups that attract electrons around this bond.Peaks at 1399 cm^{-1} and 1046 cm^{-1} belong to the C-O bonds and showed a decrease in peak strength, which is not completely lost, indicating that the oxygen group remains in the structure (Ren et al, 2011, Thakur et al, 2015).

Figure 4.25 : FTIR spectra of a. pH3 reference ve b. pH3 hydrazine.

Figure 4.26 shows FTIR spectrum of single coagulation sample. In spectra, an increase in the peaks of the oxygen-containing groups and a peak at 652 cm^{-1} (Infrared Spectroscopy Table, 2017), which is believed to correspond to the C-Cl bond stretching were observed.The reason for the rise in the peaks may be salt crystals, which are seen in the SEM analysis. Large OH peaks ranging from 3000-3500 cm^{-1} are also known as moisture peaks, and it is possible that the salt crystals adsorb water. In the reduced specimen, it is thought that newly added ions, such as decreasing peak heights due to the disappearance of oxygen-bonded groups, caused the structure to become polarized and led to stronger bonds (Konios et al, 2014).

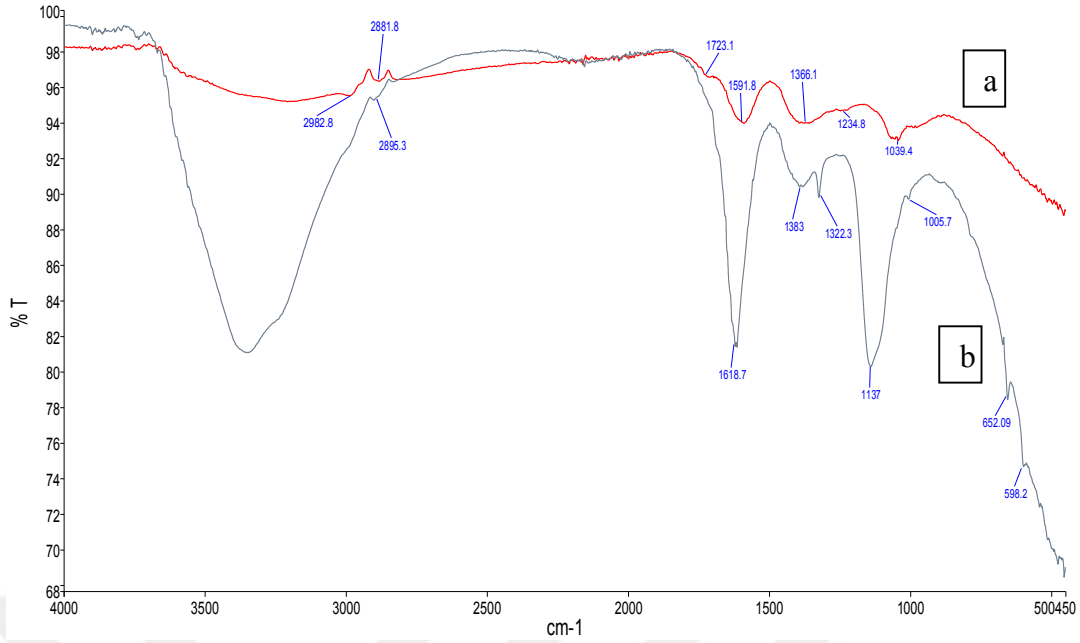

Figure 4.26 : FTIR spectra of a. pH3 reference ve b. pH3 single coagulation.

Nearly same peaks were observed for pH5 PVA sample and reference samples (Figure 4.23 and Figure 4.27). In spectra, the broad peak between 3000- 3500 cm^{-1} belongs to the O-H bond stretching in the hydroxyl group, the peaks at 2916 $cm^{-1}$and 2849 cm^{-1} belong to the stretching vibrations of symmetric and antisymmetric CH_2, respectively. The weak peak at 1715 cm^{-1} belongs to the C=O bond stretching of the carbonyl and carboxyl groups.The weakly visible peak at 1641 cm^{-1} was attributed to the adsorbed water(Salavagione et al, 2009). The peaks at 1425 cm^{-1}, 1375 cm^{-1}, and 1245 cm^{-1}belong to C=H bending (Hu et al, 2013), C-OH stretching bonds and acetate structures, respectively. The peak at 1089 cm^{-1} refers to C-O-C streching bond in epoxy groups and very small vibrations at 978 cm^{-1} refer to another epoxy, ether and peroxide groups in the structure (Kumar et al, 2017; Loryuenyong et al, 2013; Fernandez-Merino et al, 2010). The peak at 826 cm^{-1} belongs to out-of-plane C-H bonds (Galande et al, 2011)

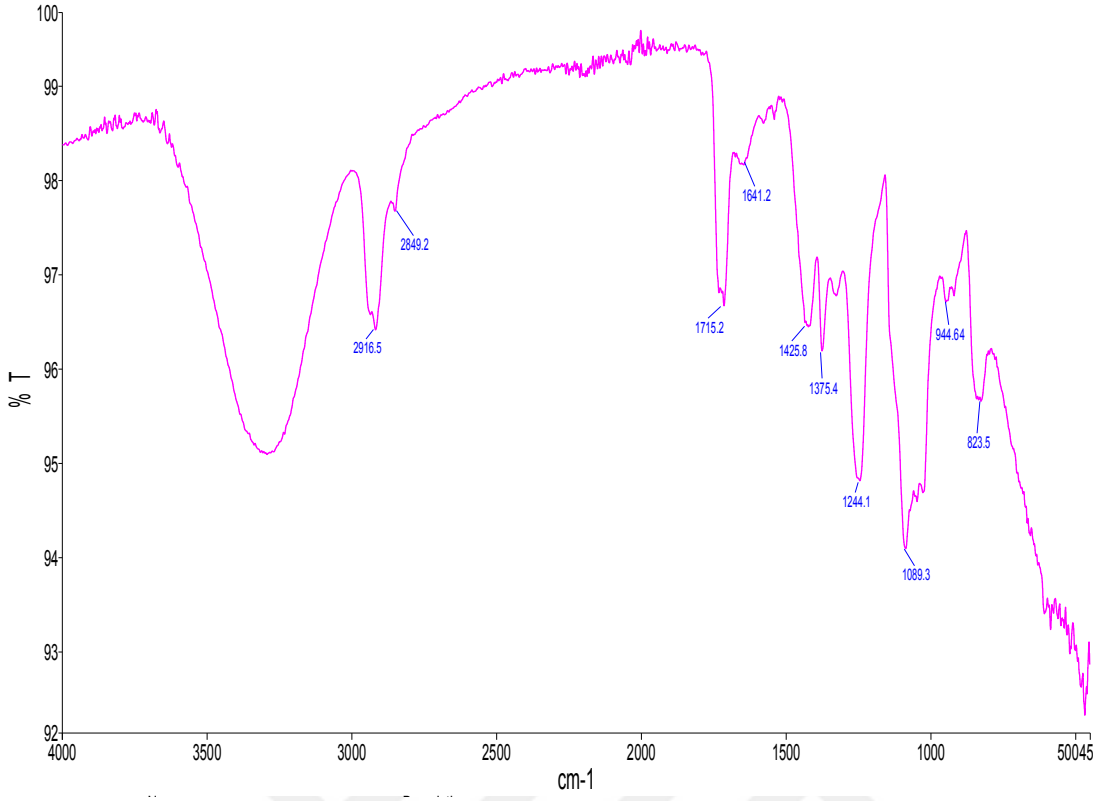

Figure 4.27 : FTIR spectra of pH5 PVA.

4.7 Raman Spectroscopy

For graphite and graphene oxide (Figure 4.28, Figure 4.29, Figure 4.33, Figure 4.34), three peaks occur in the ranges 1000–1500 cm^{-1} (D), 1500–2000 cm^{-1} (G) and 2000-2500 cm^{-1} (2D) (Drewniak et al, 2016). The D band is related to the disordered carbonaceous structure, while the G band is related to the ordered graphitic structure which is common for sp^2 carbon forms and originates from C-C bond streching (Li et al, 2017; Perumbilavil et al, 2015). The peak intensity ratio (I_D/I_G) represents the degree of graphitization of the carbon samples (Drewniak et al, 2016). The D/G intensity ratios (I_D/I_G) for these samples are shown in Table 4.5. The growth of this ratio suggests that the amount of defects increased. In the reduced sample (Figure 4.32), the I_D / I_G ratio was increased due to the loss of functional groups and formation of defects (Eigler et al, 2012; Stankovick et al, 2007). In the G band, a very small shift to the left was observed, and due to the increase of sp^2 carbon atoms, and the intensity value of the D band reduced (Perumbilavil et al, 2015).

When activated carbon is added, it is thought that carbon structure increased but disorder occured due to the settlement of active carbons in the structure and

irregularity occurred due to the formation of a curved structure in the fibers produced by single coagulation (Figure 4.30, Figure 4.31).

PVA has a characteristic peak in the range of 2900-3000 cm-1 (Wang et al. 2012). Therefore, while GO and PVA are together, the 2D peak is not sufficiently high because it is considered imprinted (Figure 4.35).

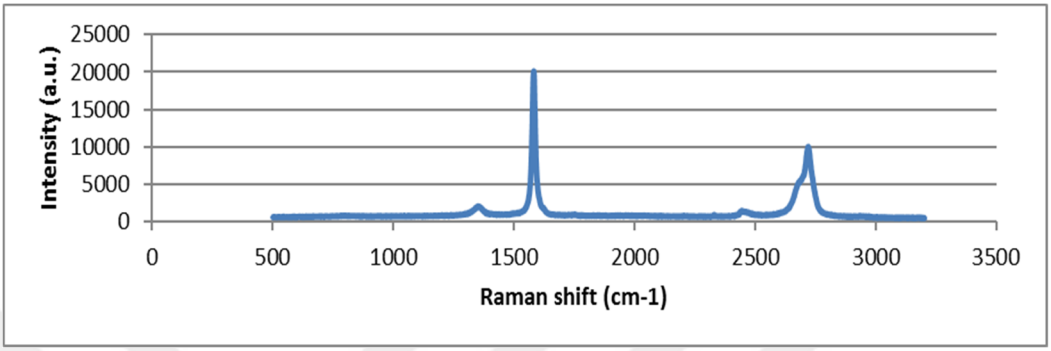

Figure 4.28 : Raman spectra of graphite (GIC).

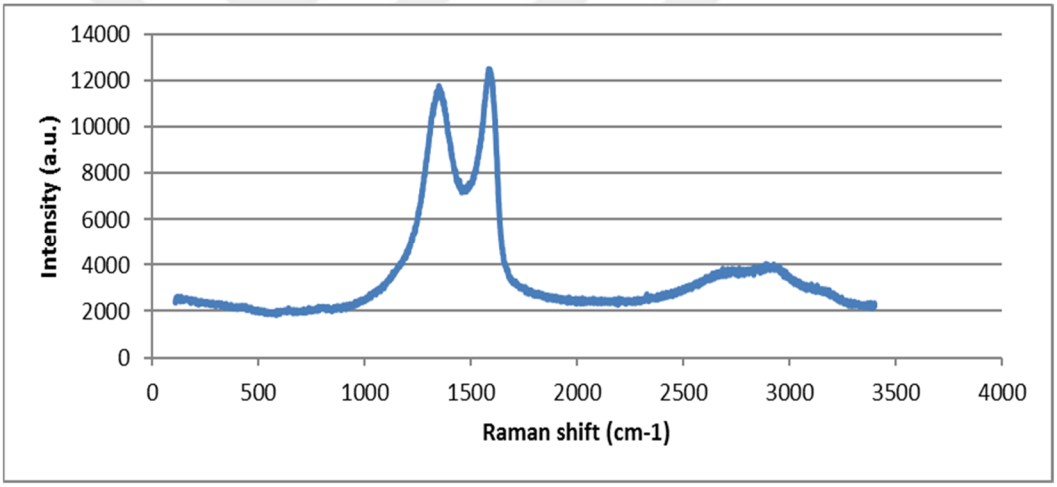

Figure 4.29 : Raman spectra of pH3 Reference.

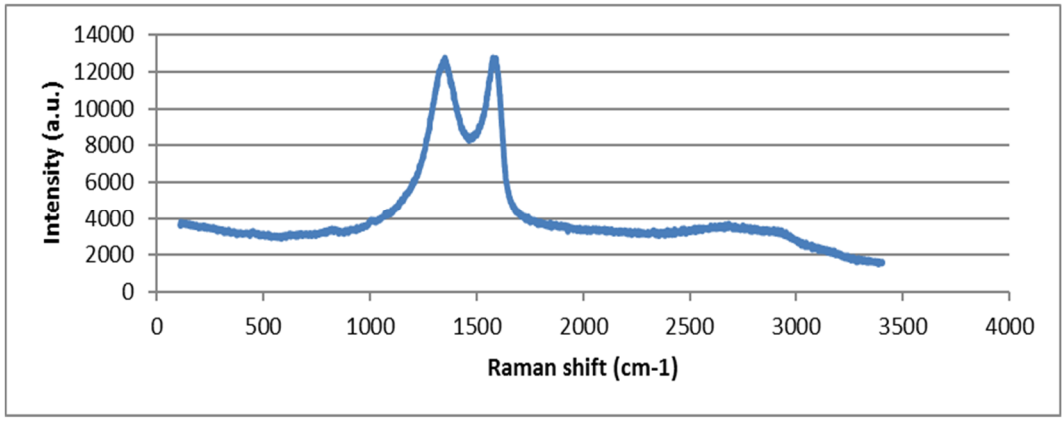

Figure 4.30 : Raman spectra of pH3 AC.

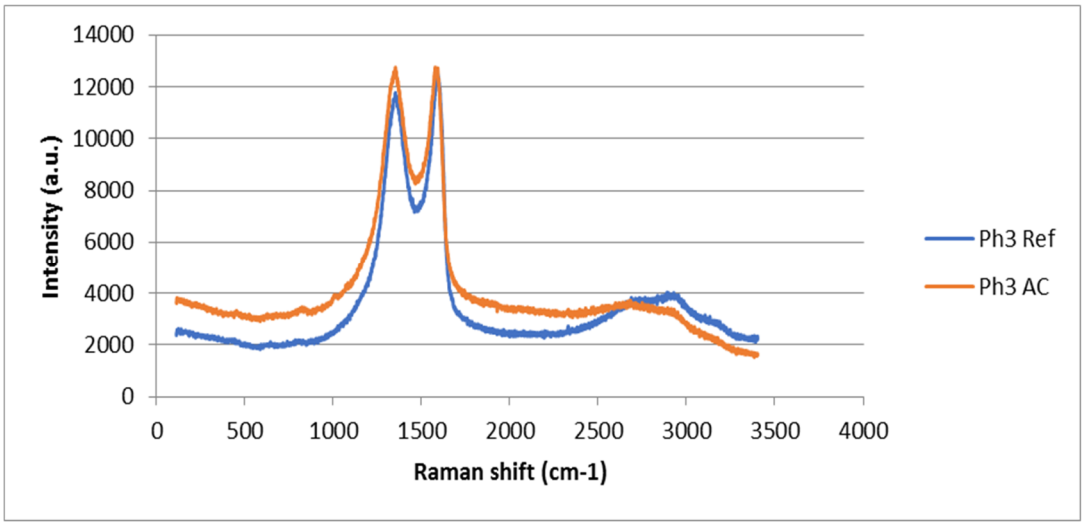

Figure 4.31 : Raman spectra of pH3 Reference and pH3 AC.

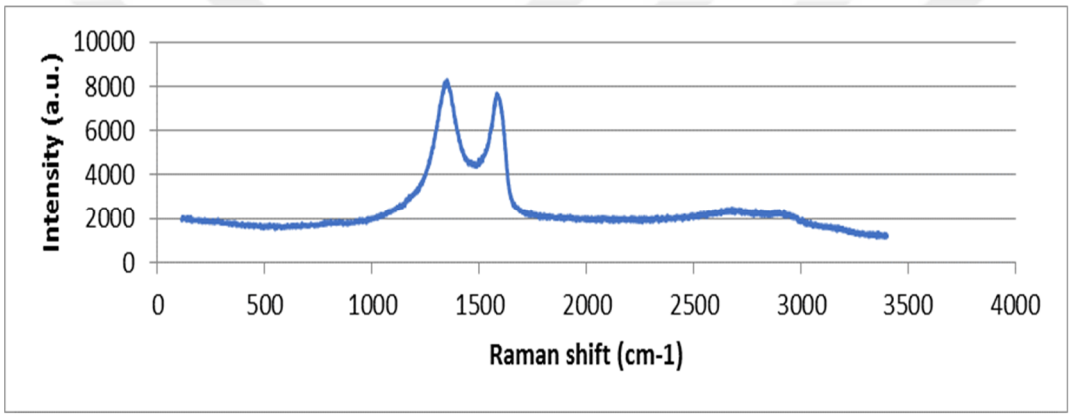

Figure 4.32 : Raman spectra of pH3 Hydrazine.

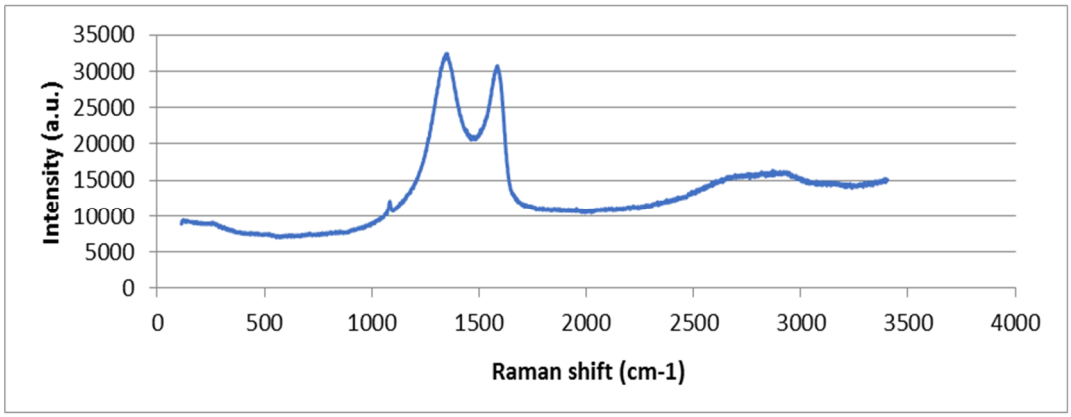

Figure 4.33 : Raman spectra of pH3 Single coagulation.

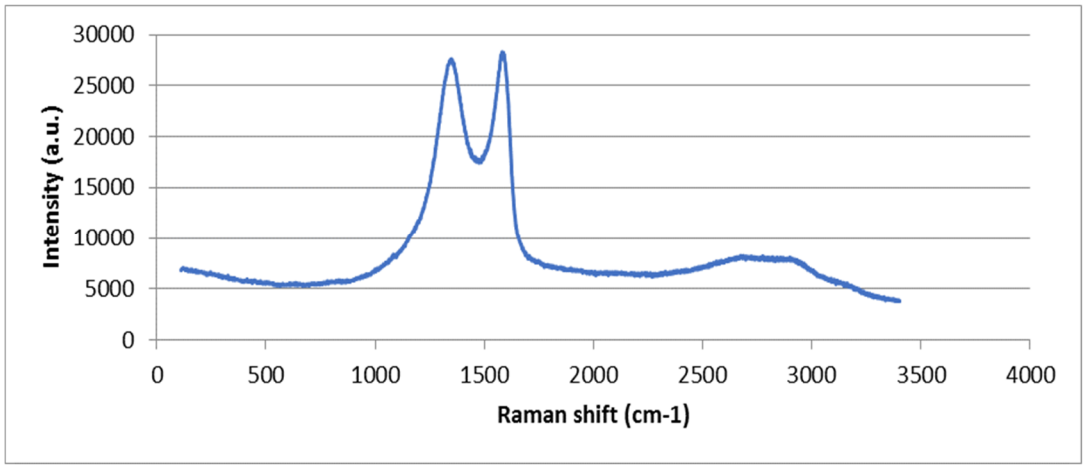

Figure 4.34 : Raman spectra of pH5 Reference.

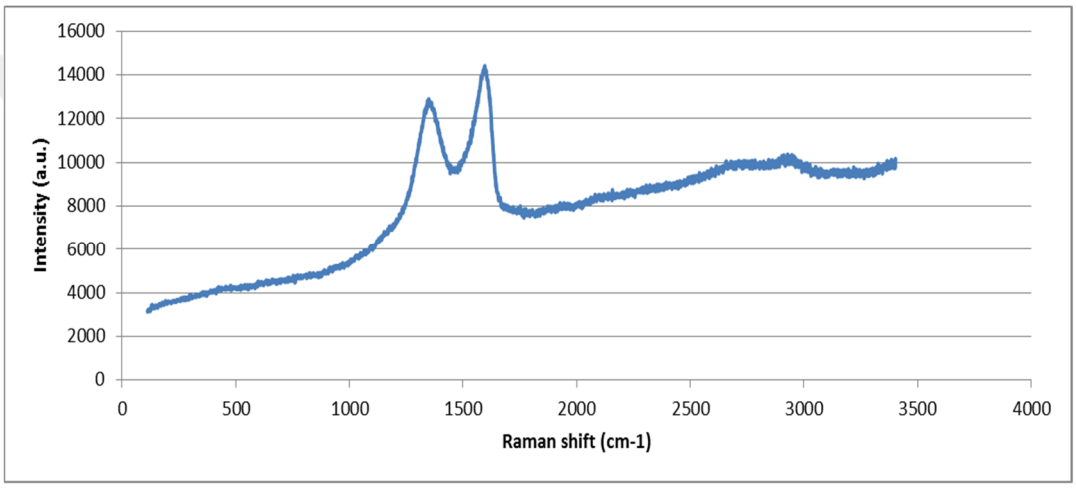

Figure 4.35 : Raman spectra of pH5 PVA.

Table 4.5 : I_D/I_G ratios.

Sample	I_D/I_G
Graphite	0.106
pH3 Reference	0.941
pH3 AC	0.999
pH3 Hydrazine	1.078
pH3 Single coagulation	1.054
pH5 Reference	0.976
pH5 PVA Reference	0,895

4.8 Thermogravimetric Analysis (TGA)

According to the TGA analysis, the loss of the water at 100 °C was observed in all samples.

As a result of the loss of the functional groups, another weight loss occurred between 150 and 250 ºC (Liu et al, 2012). While there was a weight loss of about 20% around 100 °C; approximately 46% weight loss was observed when it reaches around 250 ºC. As mentioned in previous studies (Wu et al, 2012; Kumar and Khandelwal, 2014) weight loss between 150 and 250 ºC is due to degradation of oxygenated functional groups (Figure 4.36).

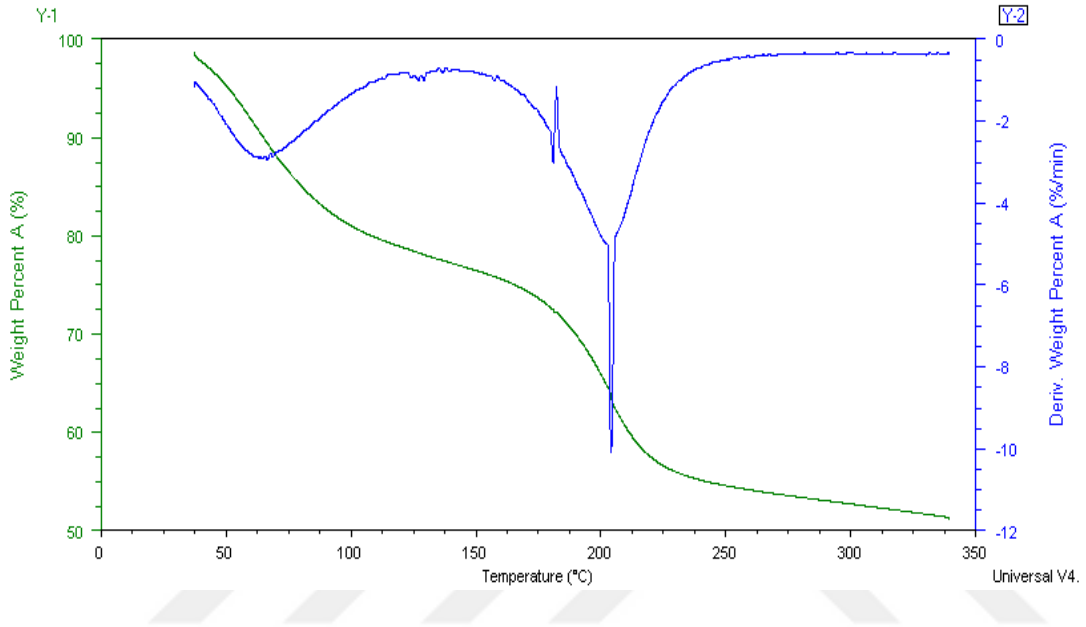

Figure 4.36 : TGA curve of pH3 reference.

Figure 4.37 shows loss of weight about 11% removal of the water around 100 °C for the pH 3 AC sample; Approximately 30% weight loss is observed when it reaches around 250 ºC.

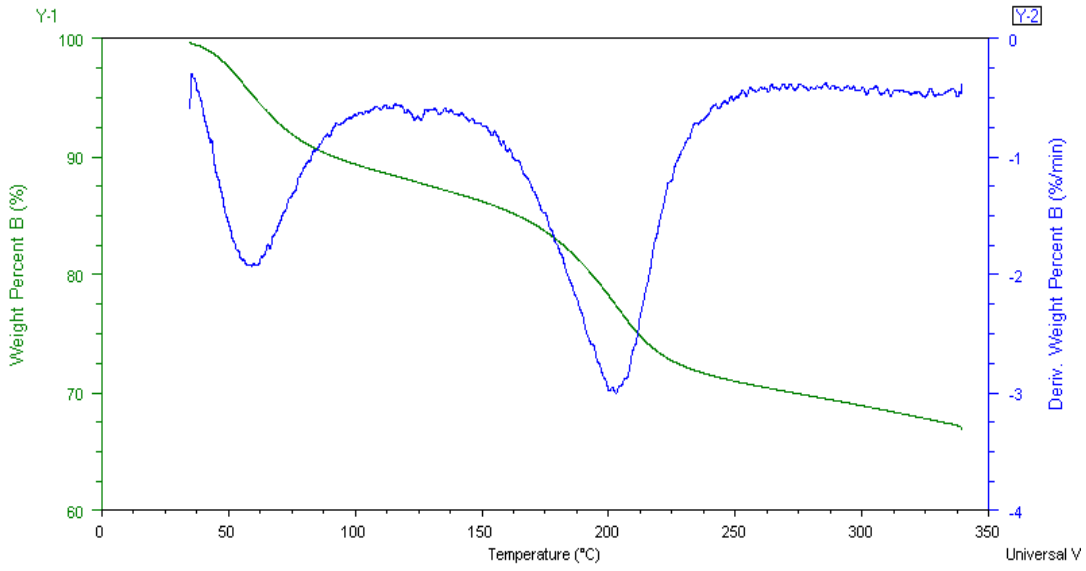

Figure 4.37 : TGA curve of pH3 AC.

Figure 4.38 shows loss of weight about 9% removal of the water around 100 °C for the pH3 hydrazine sample; Approximately 11% weight loss is observed when it reaches around 160ºC.When the reduced sample was subjected to drying to remove hydrazine residues after reduction, the loss of moisture was calculated less than the others. However, the reduced sample is thermally more stable than the graphene oxide fibers because it is largely removed from the oxygenated groups (Loryuenyong et al, 2013; Wu et al, 2012; Aldosari et al, 2013)

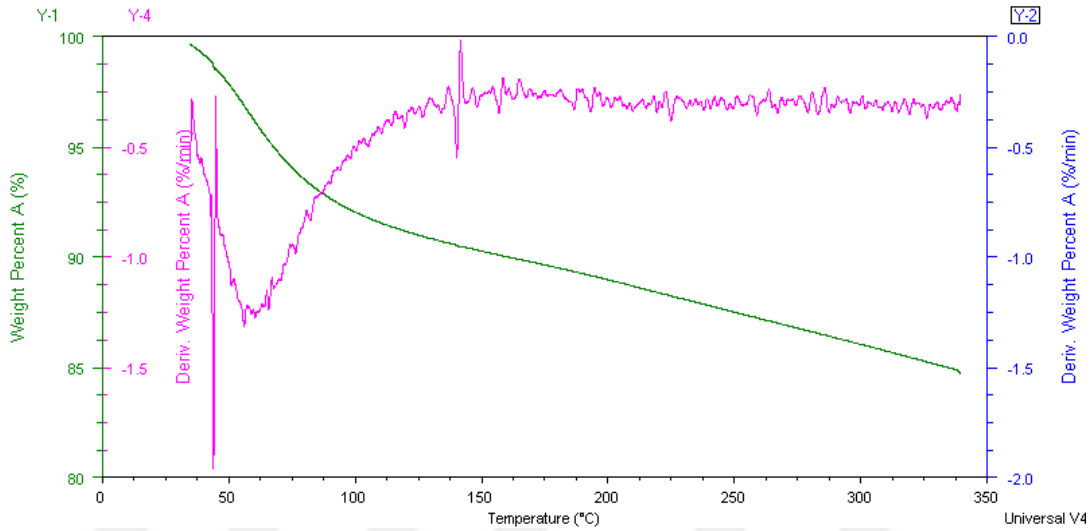

Figure 4.38 : TGA curve of pH3 hydrazine.

As seen from Figure 4.39, loss of weight about 36% removal of the water around 100 °C for the pH3 single coagulation sample. Approximately 49% weight loss is observed when it reaches around 200 ºC.

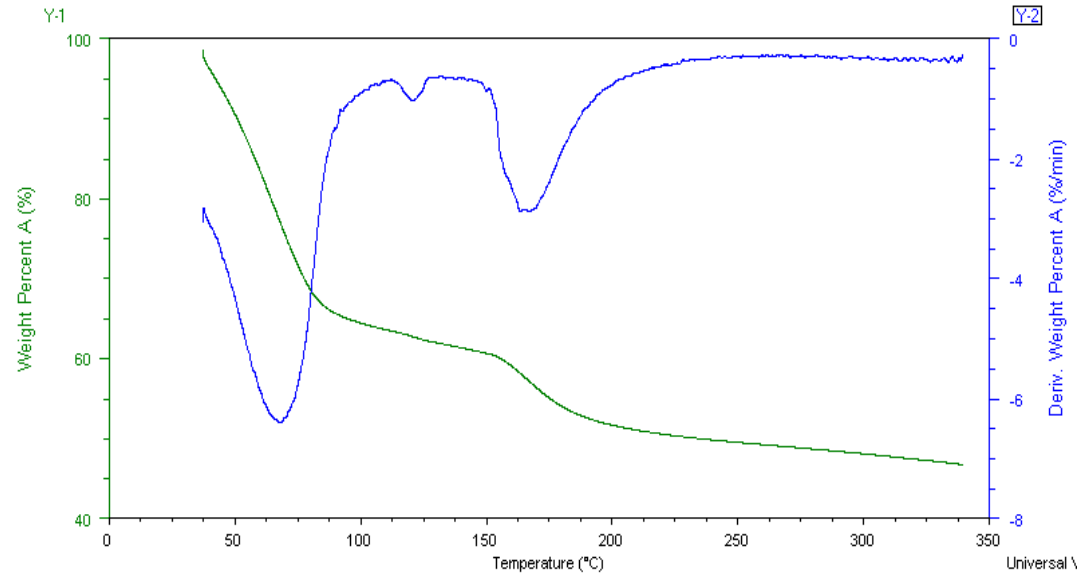

Figure 4.39 : TGA curve of pH3 single coagulation.

As seen from Figure 4.40, loss of weight about 19% removal of the water around 100 °C for the pH5 reference sample; approximately 45% weight loss is observed when it reaches around 260 ºC.

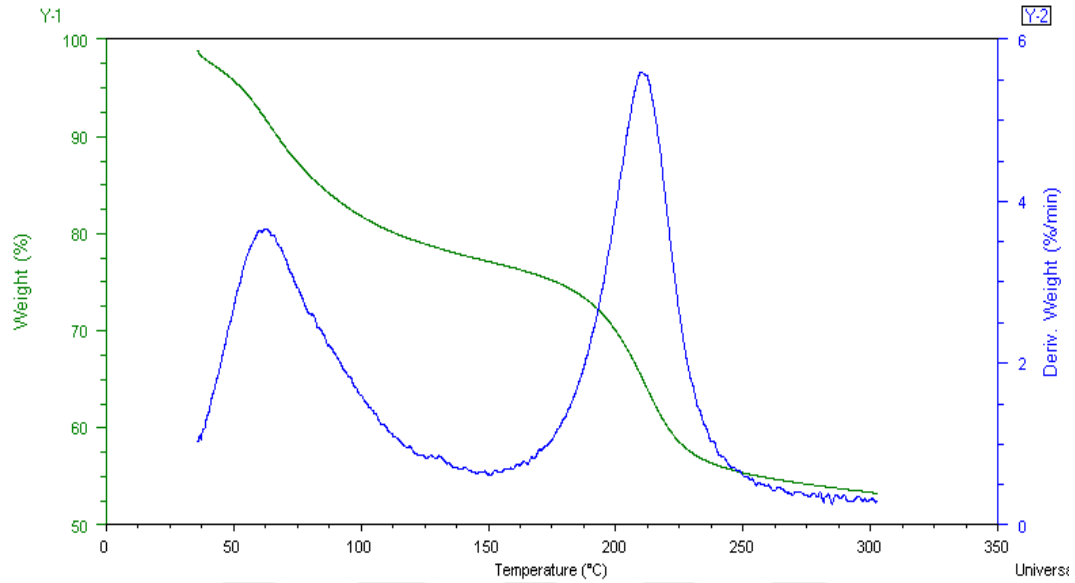

Figure 4.40 : TGA curve of pH5 reference.

As seen from Figure 4.41, loss of weight about 10% removal of the water around 100 °C for the pH5 PVA. Approximately 27% weight loss is observed when it reaches around 225ºC.

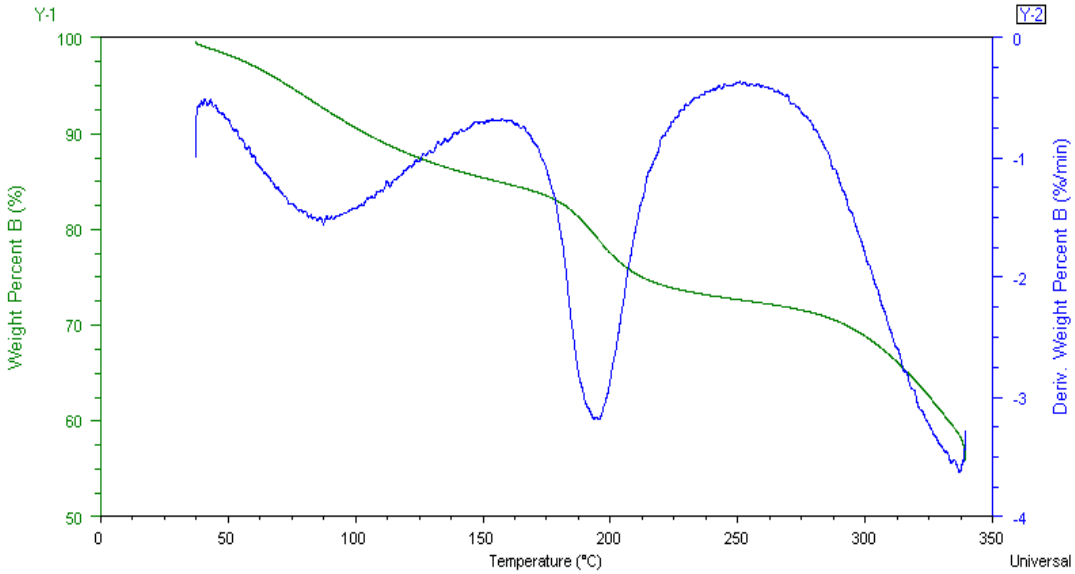

Figure 4.41 : TGA curve of pH5 PVA.

4.9 Brunauer-Emmett-Teller (BET) surface area analysis

When the results of the BET analysis given in Table 4.6 are examined, it is seen that the largest pore diameter in the pH3 group is measured for the activated carbon sample. The BET surface area is also higher than the other pH3 group samples. One of the reasons for the high adsorption of the activated carbon sample is its porous structure as we confirmed in the results. In PVA coated sample, all values including BET surface area decreased. This can be caused by the coating of the voids of the PVA.

Table 4.6 : Surface area values of fibers.

Sample	BET surface area (m^2/g)	Average pore diameter (nm)	Total pore volume (cc/g)
pH3 Reference	25.697	2.189	$2.81*10^{-2}$
pH3 AC	36.640	9.44	$8.648*10^{-2}$
pH3 Hydrazine	26.409	8.578	$5.663*10^{-2}$
pH3 Single coagulation	26.322	5.778	$3.80*10^{-2}$
pH5 Reference	24.971	5.399	$3.37*10^{-2}$
pH5 PVA	7.056	1.128	$1.99*10^{-2}$

5. ADSORPTION OF SULFUR DIOXIDE ON GO FIBERS

5.1 Production of GO Nonwoven Structure

The fibers which were produced by wet spinning method were placed in an empty container of 3.2 cm diameter to cover the entire substrate. Drying process was done in room conditions. The produced nonwoven surface (weights should not be less than 0.1 gram) conforms to other processes and tests (Figure 5.1).

Figure 5.1 : Nonwoven surface.

5.2 Production Of Reduced Nonwoven Surface

Reduction was carried out by dipping nonwoven surface into hydrazine hydrate (N_2H_5OH) solution. For this process, 15 mL of hydrazine hydrate was placed on the petri dish and placed in the samples and allowed to interaction for 20 minutes. Before subjecting to the SO_2 absorption test, the nonwoven surface was dried at 80 °C for 2h to evaporate the residual hydrazine. Volume swelling was observed on the surface (Figure 5.2).

a. 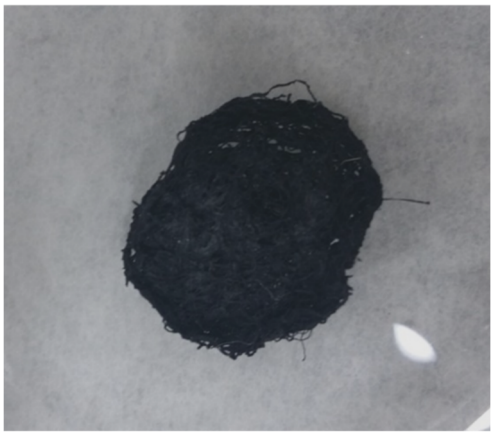 b. 

Figure 5.2 : Nonwoven surfaces a. Non-reduced surface, b. reduced surface.

5.3 SO_2 Adsorption Process

Adsorption process consists of three successive stages: Adsorption, desorption, and titration. Adsorption and desorption experiments were carried out in a tube furnace (Protherm) and throughout these stages, N_2 gas was fed to the medium in order to feed SO_2 to the system at the desired concentration and to provide an inert environment (Figure 5.3).

Figure 5.3 : Adsorption and desorption test setup.

Adsorption: The sample in the quartz tube inside the tube furnace was placed perpendicular to the incoming gas stream. Subsequently, the tube was fed with N_2 gas at 150 mL/min flow rate and SO_2 gas at 1.47 mL/min flow rate during one hour.

Desorption: Feeding of 150 mL/min N_2 gas was continued. The SO_2 gas was turned off. For a while, the N_2 gas feed was continued without processing to allow SO_2 to move away from the medium. Desorption was carried out by keeping the oven at 360

°C for 60 minutes after reaching 360 °C at a rate of 5 °C / min and, thereby releasing the sulfur dioxide trapped by the sample. The gas leaving the sample was trapped by a gas-flushing bottle placed in the gas outlet line and containing 5% of a 100 mL H_2O_2 solution. Here, SO_2 reacted with water to form H_2SO_4. The amount of sulfuric acid formed after desorption of the SO_2 gas was determined by titration.

Titration: The amount of H_2SO_4 which present in the solution after desorption process is determined by titration method and the amount of SO_2 adsorbed by the sample is calculated by molar calculation method.During the titration, 0.1 N H_2SO_4 and 0.1 N sodium hydroxide (NaOH) were used for the calibration. In addition, 0.1 N NaOH was used for titration of the H_2O_2solution. A 1 mL pipette scaled in 0.01 mL increments was used to increase the sensitivity of the assay. The volume of NaOH solution titrating the H_2O_2 solution relative to the amount of NaOH solution titrating H_2SO_4 was proportioned and the SO_2 adsorption capacity is determined.

Calculations: There are 0.05 mol H_2SO_4 in 1 liter of 0.1 N H_2SO_4 solution. Molar weight of sulfuric acid (H_2SO_4) is 98 g/mol and a mass of 0.05 mol H_2SO_4 of 98 g / mol * 0.05 mol = 4.9 g.For calibration, 3 mL of 0.1 N H_2SO_4 solution was used. In a 1 liter 0.1 N H_2SO_4 solution, there are 4.9 g H_2SO_4 and in a 3 mL H_2SO_4 solution there is 4.9 * (3/1000) = 0.0147 g H_2SO_4.In theory, 3 mL of NaOH is consumed for 3 mL of H_2SO_4, but in our experiment, 3.045 mL of NaOH solution has consumed. Further calculations are shown below;

0.0147 g H_2SO_4	3 mL NaOH
x	3.045 mL NaOH

x = 0.01492 gH_2SO_4

For 1 mL 0.1 N=4.8998 mg

Calibration showed that 1 mL NaOH solution gave neutralization reaction with the solution containing 4.8998 mg H_2SO_4. 3 mL of solution was taken from the H_2O_2 solution and it was diluted with 10 mL of water, then phenol red indicator was added. During the titration, 0.45 mL of a 0.1 N NaOH solution was used for pH3 reference sample. Next calculations were done exemplified out of pH3 reference.

1 mL 0.1 N NaOH 4.8998 mg H_2SO_4

0.45 mL x

x = 2.205 mg H_2SO_4 (3 mL of solution)

3 mL desorption solution2.205 mg H_2SO_4

100 mL desorption solution x

x = 73.5 mg H_2SO_4/ 100 mL solution

The weight of pH3 reference was 0.1540 g.

0.1540 g sample 73.5 mg H_2SO_4

1 g ssample x

x = 477.27 mg H_2SO_4/ 1 g of sample

Molar mass of H_2SO_4= 98 mg and molar mass of SO_2= 64 mg ;

98 mg H_2SO_4 64 mg SO_2

477.27 mg H_2SO_4 x

x =311.69 mg SO_2 / 1 g of sample

Calculations for each sample were made in the same way. The maximum SO2 adsorption capacities of the prepared samples were calculated by titration after desorption. Calculated SO_2 adsorption capacities are given in Table 4.7.

Table 4.7 : SO_2 adsorption capacity of fibers.

Sample	Weight (g)	The used volume of NaOH in the titration (mL)	SO_2 adsorption capacity (mg SO_2/1 g ofsample)
pH3 Reference	0.154	0.45	311.69
pH3 AC	0.125	1.05	896
pH3 Hydrazine	0.122	0.31	270.58
pH3 Single coagulation	0.385	1.37	379.17
pH5 Referece	0.332	1	320.90
pH5 PVA	0.170	0.385	369.36

According to the results in Table 4.7; the presence of active carbon has significantly increased the SO_2 adsorption capacity. Due to the reduction of functional groups which can be bonded with SO_2 by hydrazine reduction, the amount of adsorbed

SO_2also diminished.It was expected that the interaction of basic amine group with this acidic gas would give higher adsorption capacity. But nitrogen element was seen in EDS but this structure was not found in FTIR (Ünveren et al, 2017). it is understood that the reduction of functional groups is more important in the negative effect on SO_2 adsorption.For single coagulation sample, SO_2 adsorption partially increased. It has been found that with activated carbon addition provided more SO_2 adsorption capacity, because of high surface area of activated carbon. In general, pH3 reference provided SO_2 adsorption close to pH5 reference.

5.4 Energy-dispersive X-ray Spectroscopy (EDS)

Elemental composition is analyzed by Zeiss Ultra Plus Field Emission Scanning Electron Microscope at an acceleration voltage of 15 kV.

EDS analysis were made on the fibers before and after the SO_2 adsorption test.From Figure 5.4 to Figure 5.9 show the EDS results of the fibers. In nearly all samples, C, O and Ca elements were found. In addition, the concentration of carbon element in activated carbon increased, N element was observed for reduced sample and also C/O ratio increased.For single coagulation bath, the ratio of Ca and Cl is quite high as expected due to non-washed fibers. The sulfur element was seen in all samples after the adsorption, but ratios were not matching adsorption results. For example, there are differences even in multiple results from different sites. For this reason, it is difficult to get a definite result about the element rates.

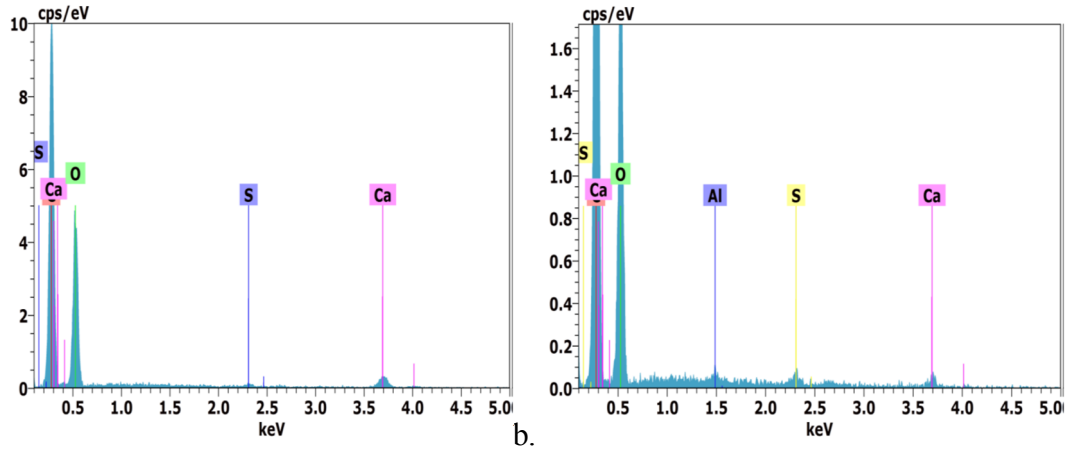

a. b.

Figure 5.4 : EDS spectrum of pH3 reference sample a. before SO_2 adsorption, b. after SO_2 adsorption.

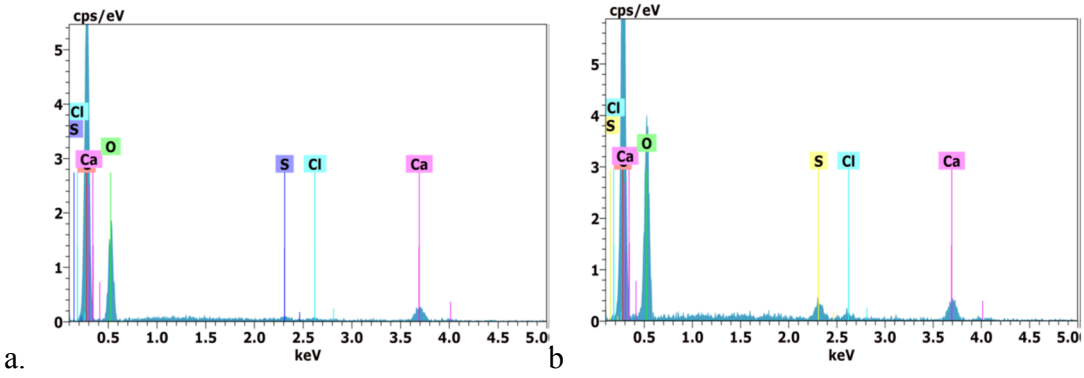

Figure 5.5 : EDS spectrum of pH3 AC sample a. before SO_2 adsorption, b. after SO_2 adsorption.

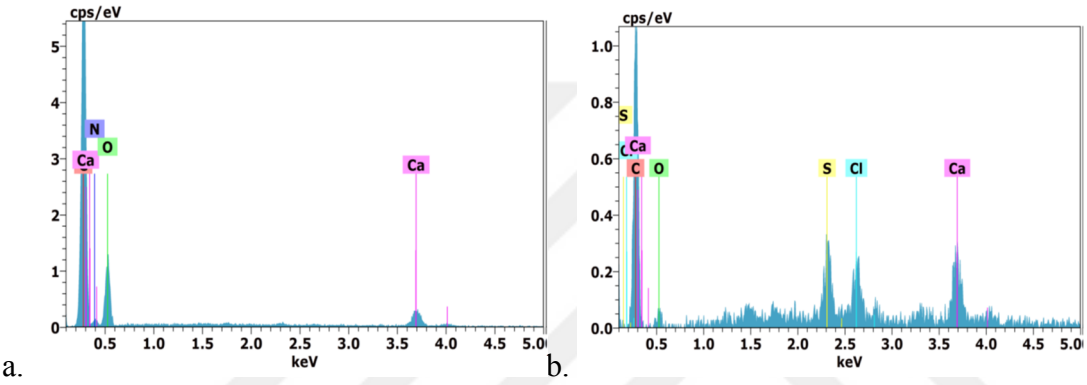

Figure 5.6 : EDS spectrum of pH3 hydrazine sample a. before SO_2 adsorption, b. after SO_2 adsorption.

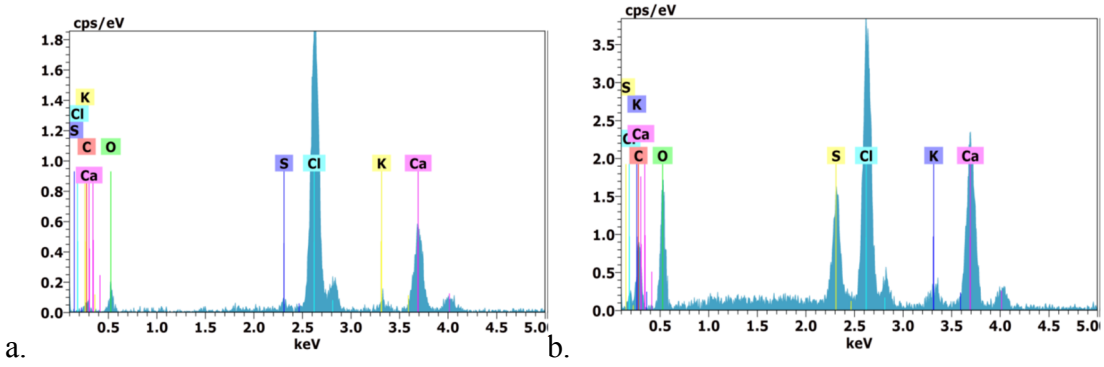

Figure 5.7 : EDS spectrum of pH3 single coagulation sample a. before SO_2 adsorption, b. after SO_2 adsorption.

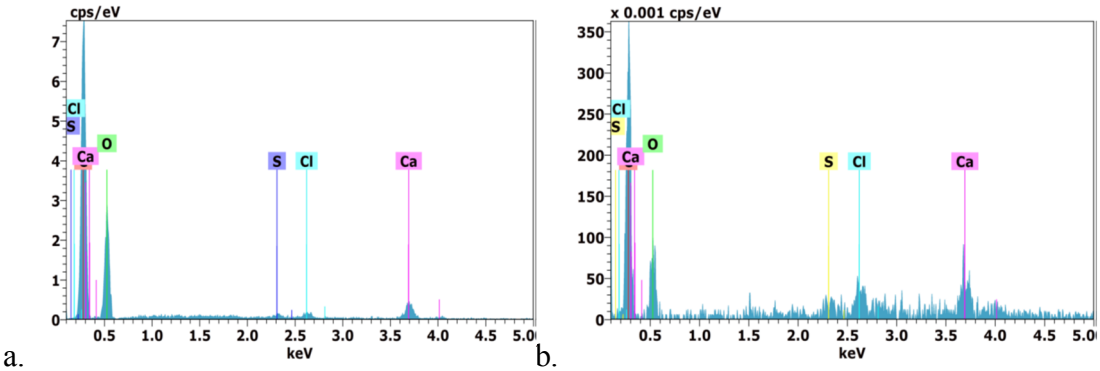

a. b.

Figure 5.8 : EDS spectrum of pH5 reference sample a. before SO_2 adsorption, b. after SO_2 adsorption.

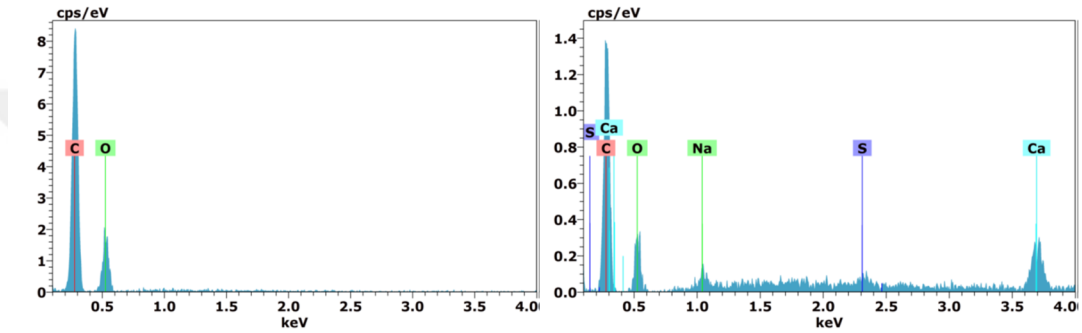

.

Figure 5.9 : EDS spectrum of pH5 PVA sample a. before SO_2 adsorption, b. after SO_2 adsorption.

When the element proportions before adsorption (Table 4.8 and Table 4.9) and the element proportions after adsorption (Table 4.10 and Table 4.11) are taken into consideration, it is observed that the S element ratio after the adsorption test was increased.

Table 4.8 : Atomic percentages of elements before adsorption.

Sample	C	O	S	Ca	Cl	N	Mn	K
pH3 Reference	56.64	39.56	0.09	0.74	-	-	-	-
pH3 AC	67.68	31.23	0.16	1.02	0.10	-	-	-
pH3 Hydrazine	72.14	25.76	-	1.28	-	0.82	-	-
pH3 Single coagulation	22.91	23.70	1.11	9.13	42.09	-	-	1.05
pH5 Reference	64.88	33.61	0.14	1.15	0.22	-	-	-
pH5 PVA	74.71	25.29	-	-	-	-	-	-

Table 4.9 : Weight percentages of elements before adsorption.

Sample	C	O	S	Ca	Cl	N	Mn	K	C/O
pH3 Reference	51.88	45.83	0.21	2.07	-	-	-	-	1.075
pH3 AC	59.60	36.74	0.39	3.01	0.27	-	-	-	1.622
pH3 Hydrazine	64.40	30.73	-	3.82	-	0.86	-	-	2.096
pH3 Single coagulation	10.63	14.65	1.37	14.14	57.62	-	-	1.59	0.726
pH5 Reference	56.66	39.10	0.33	3.34	0.57	-	-	-	1.449
pH5 PVA	68.92	31.08	-	-	-	-	-	-	2.22

Table 4.10 : Atomic percentages of elements after adsorption.

Sample	C	O	S	Ca	Cl	Na	Mn	K	Al	Si
pH3 Reference	61.91	37.63	0.12	0.26	-	-	-	-	0.08	-
pH3 AC	61.88	36.57	0.44	0.95	0.15	-	-	-	-	-
pH3 Hydrazine	86.95	4.67	2.68	3.27	2.44	-	-	-	-	-
pH3 Single coagulation	38.62	36.25	3.31	9.42	11.53	-	-	0.87	-	-
pH5 Reference	71.39	24.08	0.80	2.42	1.31	-	-	-	-	-
pH5 PVA	59.38	23.77	0.89	9.52	-	6.44	-	-	-	-

Table 4.11 : Weight percentages of elements after adsorption.

Sample	C	O	S	Ca	Cl	Na	K	Al	Si	C/O
pH3 Reference	54.59	44.20	0.28	0.77	-	-	-	0.16	-	1.235
pH3 AC	53.61	42.21	1.03	2.75	0.40	-	-	-	-	1.270
pH3 Hydrazine	73.44	5.25	6.03	9.21	6.08	-	-	-	-	13.989
pH3 Single coagulation	23.54	29.44	5.38	19.16	20.74	-	1.73	-	-	0.799
pH5 Reference	60.74	27.29	1.83	6.86	3.29	-	-	-	-	2.226
pH5 PVA	43.19	23.03	1.73	23.09	-	8.96	-	-	-	1.88

6. CONCLUSIONS

In this study, graphene oxide was synthesizedby Hummers method and then two different pH groups of samples(pH3 and pH5) were produced. To see the effect of some operations, reduction procedure by hydrazine hydrate, activated carbon addition, PVA coating and single coagulation bath application were tried on GO fibers. Characterization of GO fibers was carried out by SEM and AFM, also other qualitative and quantitative analyses like XRD, FTIR, Raman, conductivity and tex number were performed. TGA was used to characterize the thermal properties of fibers and most importantly the surface areas of fibers were calculated by BET analysis.

In acidic pH value (pH3) the fiber stiffness was increased too much, there were much more fiber breaks compared to pH5 and the electrical conductivity was lower. In the samples with pH5, lower interlayer distance and higher crystal size were observed than samples with pH3.

Raman analysis of pH3 group and pH5 group fiber samples showed D band at 1000-1500 cm-1, G band at 1500-1500 cm-1 and 2D band at 2500-3000 cm-1.

In the EDS analysis, it was seen that the C/O ratio of pH3 fibers was slightly lower than the pH5 fibers.

On the GO fibers, hydrazine hydrate reduction studies have been carried out. With the reduction, the fibers have a swollen, voided and defective structure. At the same time, the surface roughness increased in the AFM test.Because of the reduction, the peak about 26 degrees has appeared with an interlayer distance of 3.34 Å in the XRD pattern by the reason of reduction of oxygenated groups and occurring a similar structure of graphite.With PVA coating the irregularity of the structure decreased as can be seen in SEM and AFM analyses.

The fibers produced with single bath (sudden coagulation) have a higher electrical conductivity (10^{-2} S/cm), compared to multiple baths, the surface roughness is higher, and all products are in the semiconductor range. Due to the use of a single bath on the fiber produced and the $CaCl_2$ salt in that bath, crystal structures remained

on the fiber and in EDX analysis it was understood that these crystal structures were originated from "Ca".On the other hand, the C / O ratio decreased with sudden coagulation.

Finally, SO_2 adsorption tests were performed on GO fibers and the nonwoven surface was produced. After SO_2 adsorption, the EDX analysis revealed that the "S" element ratio increasedon all non-woven surfaces. It was found that the nonwoven surfaces composed of pH3 and pH5 fibers had close SO_2 adsorption capacity (310-320 mg SO_2/1 g of sample), however nonwoven structure produced by activated carbon doped GO fiber has 3 times higher SO_2 adsorption capacity than reference GO fiber. The BET analysis also showed that the highest surface area beongs to AC fibers. With the single coagulation process, the adsorption capacity is slightly increased (around 380 mg SO_2/1 g of sample), which is partly due to increasing functional groups. SO_2 adsorption capacity decreased by hydrazine reduction. Slightly higher SO_2 adsorption was achieved due to PVA (369 mg SO_2 /1 g of sample).

REFERENCES

Aldosari M. A., Othman A. A., & Alsharaeh E. H. (2013). Synthesis and Characterization of the in Situ Bulk Polymerization of PMMA Containing Graphene Sheets Using Microwave Irradiation, *Molecules, 18*, 3152-3167.

Allen M. J., Tung V. C., & Kaner R.B. (2010). Honeycomb Carbon: A Review of Graphene, *Chem. Rev, 110* (1), 132–145.

Babu D. J., Kühl F. G., Yadav S., Markert D., Bruns M., Hampeb M. J. & Schneider J. J. (2016). Adsorption of pure SO2 on nanoscaled graphene oxide. *Royal Society of Chemistry Adv., 6,* 36834-36839.

Bakry, R., Vallant, R. M., Najam-ul-Haq, M., Rainer, M., Szabo, Z., Huck, C. W., & Bonn, G. K. (2007). Medicinal applications of fullerenes, *International Journal of Nanomedicine, 2* (4), 639–649.

Blanton T., & Majumdar D. (2012). X-ray diffraction characterization of polymer intercalated graphite oxide, *JCPDS-International Centre for Diffraction Data, 27* (2), 104-107.

Chen C. Xu K., Miao L. & Jiang J. (2014). Enhanced adsorption of acidic gases (CO_2, NO_2 and SO_2) on light metal decorated graphene oxide. *Phys. Chem. Chem Phys., 16*, 11031-11036.

Chen W. & Yan L. (2011). In situ self-assembly of mild chemical reduction graphene for three-dimensional architectures, *Nanoscale, 3* (8), 3132–3137.

Chiu N., Huang T. & Lai H. (2013). Advances in Graphene Science. *Graphene Oxide Based Surface Plasmon Resonance Biosensors* (Vol. 8, pp. 191-216). Intech.

Cividanes L.S. & Thim G. P. (2016). *Functionalizing Graphene and Carbon Nanotubes A Review*. Switzerland: Springer.

Cong, H.-P, Ren, X.-C., Wang, P., Yu, S.-H. (2012). Wet-spinning assembly of continuous, neat, and macroscopic graphene fibers, *Sci. Rep. 2* (613), 1-6.

Dimiev A. M. & Eigler S. (2017). *Graphene Oxide Fundamentals and Applications.* United Kingdom: Wiley.

Dimiev A.M. & Tour J. M. (2014). Mechanism of Graphene Oxide Formation, *ACS Nano, 8* (3), 3060-3068.

Drewniak S., Muzyka R., Stolarczyk A. Pustelny T., Kotyczka-Morańska M. & Setkiewicz M. (2016). Studies of reduced graphene oxide and graphite oxide in the aspect of their possible application in gas sensors, *Sensors, 16* (103), 1-16.

Dreyer D. R., Park S., Bielawski C. W. & Ruoff R. S. (2009). The chemistry of graphene oxide, *Chemical Society Reviews, 39*, 228-240.

Dunn J. P., Stenger H. G., Wachs I. E. (1999). Oxidation of SO2 over supported metal oxide catalysts. *Journal of Catalysis, 181*, 233–243.

Eda, G., Fanchini, G. & Chhowalla, M. (2008). Large-area ultrathin films of reduced graphene oxide as a transparent and flexible electronic material. *Nat. Nanotechnol., 3*, 270–274.

Eigler S., Dotzer C.& Hirsch A. (2012). Visualization of defect densities in reduced graphene oxide*, Carbon, 50,* 3666-3673.

Electrical Conductivity of Aqueous Solutions. (2017). *Retrieved June 11, 2017, from* http://sites.chem.colostate.edu/diverdi/all_courses/CRC%20reference%20data/electrical%20conductivity%20of%20aqueous%20solutions.pdf.

Fang C. K. (2009). Mechanical and Tribological Investigations on Carbon Allotropes, *Bulletin of College of Engineering, National Ilan University, 5*, 131-167.

Fernandez-Merino, M. J., Guardia, L., Paredes, J. I., Villar-Rodil, S., Solis-Fernandez, P., Martinez-Alonso, A. & Tascon, J. M. D. (2010). Vitamin C is an ideal substitute for hydrazine in the reduction of graphene oxide suspensions. *The Journal of Physical Chemistry C, 114* (14), 6426-6432.

Ferrari A. C. (2007). Raman spectroscopy of graphene and graphite: Disorder, electron phonon coupling, doping and nonadiabatic effects, *Solid State Communications, 143*, 47–57.

Galande C., Mohite A. D., Naumov A. V., Gao W., Ci L., Ajayan A., Gao H., Srivastava A., Weisman R. B.& Ajayan P. M. (2011). Quasi-Molecular Fluorescence from Graphene Oxide, *Scientific Reports, 1* (85), 1-5.

Geim A. K. & Novoselov K. S. (2007). The rise of graphene, *Nature, 6*, 183-191.

Gökçeören A. T. (2010). *Improvement Of Thermal And Electrical Properties Of PNVCz By Copolymers And Composites.* (Doktora tezi). İstanbul Teknik Üniversitesi, Fen Bilimleri Enstitüsü, İstanbul.

Han C. D. (2007). *Rheology and Processing of Polymeric Materials* (Vol. 2, pp. 261). Oxford University Press.

Hu H., Xin J. H., Hu H., Chan A.& He L. (2013). Glutaraldehyde–chitosan and poly (vinyl alcohol) blends, and fluorescence oftheir nano-silica composite films, *Carbohydrate Polymers 91*, 305–313.

Infrared Spectroscopy Table. *(2017). Retrieved June 11, 2017, from* http://www.chem.ucla.edu/~bacher/General/30BL/IR/ir.html.

İlhan Y. (2012). *Baca gazı kükürt gidermede doğal soda külü üretim süreci atığının kullanımının araştırılması* (Master's Thesis). Ankara University, Ankara.

Kaushik B. K. & Majumder M. K. (2015). *Carbon Nanotube Based VLSI Interconnects*. Springer India.

Kashyap S., Mishra S.& Behera S. K. (2014). Aqueous Colloidal Stability of Graphene Oxide and Chemically Converted Graphene, *Journal of Nanoparticles, 2014*, 1-6.

Katsnelson M. I. (2007). Graphene: carbon in two dimensions*, Materials Today, 10* (1-2), 20-27.

Katsnelson, M. I. (2012*). Graphene Carbon in Two Dimensions*. New York: Cambridge University Press.

Kishar E. A., Ahmed D. A., Mohammed M. R.&Noury R. (2013). Effect of calcium chloride on the hydration characteristics of ground clay bricks cement pastes, *Beni-Suef University Jornal of Basic and Applied Science 2*, 20-30.

Kohno J., Mafune F.& Kondow T. (2000). Formation of Ca+ (EtOH)m from Alcohol Solutions of $CaCl_2$*, J. Phys. Chem. A, 104* (6), 1079-1084.

Konios D., Stylianakis M. M., Stratakis E.& Kymakis E. (2014). Dispersion behaviour of graphene oxide and reduced graphene oxide, *Journal of Colloid and Interface Science, Journal of Colloid and Interface Science,* 430, 108–112.

Konkena B. & Vasudevan S. (2012). Understanding Aqueous Dispersibility of Graphene Oxide and Reduced Graphene Oxide through pKa Measurements, *J. Phys. Chem. Lett., 3,* 867−872.

Kumar A. & Khandelwal M. (2014). Amino acid mediated functionalization and reduction of graphene oxide – synthesis and the formation mechanism of nitrogen-doped graphene, *New J. Chem., 38*, 3457-3467.

Kumar R., Avasthi D.K.& Kaur A., (2017). Fabrication of chemiresistive gas sensors based on multistep reduced graphene oxide for low parts per million monitoring of sulfur dioxide at room temperature, *Sensors and Actuators B: Chemical, 242*, 461–468.

Lee Y. & Park J. (2002). Adsorption Characteristics of SO_2 on Activated Carbon Prepared from Coconut Shell with Potassium Hydroxide Activation. *Environ. Sci. Technol., 36* (5), 1086-1092.

Li F., Jiang X., Zhao J. & Zhang S. (2015). Graphene oxide:A promising nanomaterial for energy and environmental applications*, Nano Emergy, 16*, 488-515.

Li Y., Shang T., Gao J.& Jin X. (2017). Nitrogen-doped activated carbon / graphene composites as high-performance supercapacitor electrodes, *RSC Adv., 7,* 19098-19105.

Lin Y., Zhang L., Mao H., Chow P., Xiao Y., Baldini M., Shu J., & Mao W. L. (2011). Amorphous Diamond: A High-Pressure Superhard Carbon Allotrope*, Phys. Rev. Lett. 107*, 175504.

Liu, Z. S. (2008). Adsorption of SO_2 and NO from incineration flue gas onto activated carbon fibers, *Waste Manag, 28* (11), 2329-2335.

Loryuenyong V., Totepvimarn K., Eimburanapravat P.,Boonchompoo W.& Buasri A. (2013). Preparation and Characterization of Reduced Graphene Oxide Sheets via Water-Based Exfoliation and Reduction Methods, *Advances in Materials Science and Engineering, 2013*, 1-5.

Malhotra1 B. D., Srivastava1 S. & Augustine S. (2015). Biosensors For Food Toxin Detection: Carbon Nanotubes And Graphene*, Mater. Res. Soc. Symp. Proc., 1725*.

Manguna C.L., DeBarrb J.A. & Economya J. (2001). Adsorption of sulfur dioxide on ammonia-treated activated carbon fibers. *Carbon, 39,* 1689–1696.

Marcu I. C. & Sandulescu I. (2004). Study of sulfur dioxide adsorption on Y zeolite. *J. Serb. Chem. Soc., 69* (7), 563–569.

Mash H. & F. R. Reinoso. (2006). *Activated Carbon*. Great Britain: Elsevier.

Mikhailov S. (2011). *Physics and Applications of Graphene – Theory*. Croatia: Intech.

Monshi A., Foroughi M. R.& Monshi M. R. (2012). Modified Scherrer Equation to Estimate More Accurately Nano-Crystallite Size Using XRD, *World Journal of Nano Science and Engineering, 2* (3), 154-160.

Morgan, P. (2005). *Carbon Fibers and Their Composites*. Boca Raton, FL.: CRC Press.

Muhamad K. S. S. K., Mohamed F., Radiman S., Hamzah A., Sarmani S., Siong K. K., Yasir M. S., Rahman I. A. & Roshli N. R. Md. (2016). Synthesis and Characterization of Exfoliated Graphene Oxide, *AIP Conference Proceedings 1784*, 1-5.

Mukhopadhyay P. & Gupta R. K. (2013). *Graphite, Graphene, and their polymer nanocomposites*. Boca Raton, FL.: CRC Press.

Nakajima T. (1994). Advanced fiber spinning technology: Woodhead.

Nirmala R., Nam K. T., Navamathavan R., Parl S.-J.& Kim H. Y. (2011). Hydroxyapatite Mineralization on the Calcium Chloride Blended Polyurethane Nanofiber via Biomimetic Method, *Nanoscale Res Lett.,6* (2), 1-8.

Park S., Hu Y., Hwang J. O., Lee E. S., Casabianca L. B., Cai W., Potts J. R., Ha H., Chen S., Oh J., Kim S. O., Kim Y.-H.& Ishi Y., Ruoff R. S. (2012). Chemical structures of hydrazine-treated graphene oxide and generation of aromatic nitrogen doping, *Nat. Commun. 3* (638), 1-8.

Pei S. & Cheng H. (2012). The reduction of graphene oxide*, Carbon, 50* (9), 3210-3228.

Perrozzi F., Prezioso S. & Ottaviano L. (2015). Graphene oxide: from fundamentals to applications, *Journal of Physics: Condensed Matter, 27*, 1-21.

Perumbilavil S., Sankar P., Rose T. P.& Philip R. (2015). White light Z-scan measurements of ultrafast optical nonlinearity in reduced graphene oxide nanosheets in the 400–700 nm region, *Applied Physics Letters, Appl. Phys. Lett. 107*, 051104.

Pierson, H. O. (1993). *Handbook of Carbon, Graphite, Diamond and Fullerenes Properties, Processing and Applications*. New Jersey, USA.: Noyes Publications.

Rao C. N. R. & Sood A. K. (2013). *Graphene: Synthesis, Properties, and Phenomena*, New York: Wiley.

Ren P., Yan D., Ji X., Chen T. & Li Z. (2011). Temperature dependence of graphene oxide reduced by hydrazine hydrate, *Nanotechnology ,22* (5), 1-8.

Salavagione H. J., Gomez M. A.& Martinez G. (2009). Polymeric modification of graphene through esterification of graphite oxide and poly(vinyl alcohol), *Macromolecules, 42* (17), 6331–6334.

Saner B., Okyay F.& Yürüm Y. (2010). Utilization of multiple graphene layers in fuel cells. 1. An improved technique for the exfoliation of graphene-based nanosheets from graphite, *Fuel, 89* (8), 1903-1910.

Sasmaz E. & Wilcox J, J. (2008). Mercury Species and SO_2 Adsorption on CaO(100). *Phys. Chem. C, 112,* 16484–16490.

Sattler, K.D. (2016). *Carbon Nanomaterials Sourcebook Volume I: Graphene, Fullerenes, Nanotubes and Nanodiamonds*. Boca Raton, FL.: CRC Press.

Seredych, M., & Bandosz, T. J. (2010). Effects of Surface Features on Adsorption of SO_2 on Graphite Oxide/$Zr(OH)_4$ Composites. *J. Phys. Chem. C, 114* (34), 14552–14560.

Seredych M., Mabayoje O. & Bandosz T. J. (2013). Involvement of water and visible light in the enhancement in SO_2 adsorption at ambient conditions on the surface of zinc (hydr)oxide/graphite oxide composites. *Chemical Engineering Journal, 223*, 442–453.

Shao L., Chen G., Yea H., Wu Y., Qiao Z., Zhu Y. & Niu H. (2013). Sulfur dioxide adsorbed on graphene and heteroatom-doped graphene: a first-principles study. *Eur. Phys. J. B, 86,* 54.

Singh D.K., Iyer P. K.& Giri P. K. (2010). Diameter dependence of interwall separation and strain in multiwalled carbon nanotubes probed by X-ray diffraction and Raman scattering studies, *Diamond & Related Materials, 19*, 1281–1288.

Stankovich S., Dikin D. A., Piner R. D., Kohlhaas K. A., Kleinhammes A., Jia Y., Nguyen S. T.& Ruoff R. S. (2007). Synthesis of graphene-based nanosheets via chemical reduction of exfoliated graphite oxide, *Carbon, 45* (7), 1558–1565.

Sun M., Wang G., Li X. & Li C. (2014). Irradiation preparation of reduced graphene oxide/carbon nanotube composites for high-performance supercapacitors, *Journal of Power Sources, 245*, 436-444.

Swanson H. E., McMurdie H. F., Morris M. C.& Evans E. H. (1974). *Standard X-ray Diffraction Powder Patterns*. Washington D.C: U.S. Government Printing Office.

Tan K., Canepa P., Gong Q., Liu J., Johnson D. H., Dyevoich A., Thallapally P. K., Thonhauser T., Li J., & Chabal Y. J. (2013). Mechanism of preferential adsorption of SO_2 into two microporous paddle wheel frameworks M (bdc)(ted) 0.5. *Chemistry of Materials, 25,* 4653−4662.

Thakur A., Kumar S.& Rangra V. S. (2015). Synthesis of reduced graphene oxide (rGO) via chemical reduction, *AIP Conference Proceedings, 1661* (1), 080032.

Tseng H. & Wey M. (2004). Study of SO2 adsorption and thermal regeneration over activated carbon-supported copper oxide catalysts. *Carbon, 42* (11), 2269-2278.

Ucar, N., Cavdar, Z., Karatepe, N., Altay, P., Kızıldag, N. (2016). SO2 Adsorption Capability Of Activated Carbon Nanofibers Produced By Different Activation Process Parameters. *Tekstil Ve Konfeksiyon, 26* (4), 407-413. Retrieved from http://dergipark.gov.tr/tekstilvekonfeksiyon/issue/27038/284604.

Uhl F. M., Yao Q., Nakajima H., Manias E. & Wilkie C. A. (2005). Expandable graphite/polyamide-6 nanocomposites, *Polymer Degradation and Stability, 89,* 70-84.

Uriarte L. M., Dubessy J., Boulet P., Baonza V. G., Bihannic I.& Robert P. (2015). Reference Raman spectra of synthesized $CaCl_2$.nH2O solids (n= 0, 2, 4, 6*), J. Raman Spectrosc., 46* (10), 822–828.

Ünveren E. E., Monkul B. Ö., Sarıoğlan Ş., Karademir N. & Alper E. (2017). Solid amine sorbents for CO_2 capture by chemical adsorption: A review, *Petroleum, 3* (1), 37-50.

Valapa R. B., Pugazhenthi G. & Katiyar V. (2015). Effect of graphene content on the properties of poly(lactic acid) nanocomposites, *RSC Advances, , 5* (36), 28410–28423.

Wang C., Li Y., Ding G., Xie X.& Jiang M. (2012). Preparation and Characterization of Graphene Oxide/Poly(vinyl alcohol) Composite Nanofibers via Electrospinning, *Journal of Applied Polymer Science, 127* (4), 3026-3032.

Wu T., Wang X., Qiu H., Gao J., Wang W.& Liu Y. (2012). Graphene oxide reduced and modified by soft nanoparticles and its catalysis of the Knoevenagel condensation, *J. Mater. Chem., 22*, 4772–4779.

***XRD Pattern**. (2017). Retrieved July 13, 2017, from http://www.cee.mtu.edu/~krpeters/Ca-oxy-movies/cacl2pptdry.jpg.*

Yang Y., Asiri A. M., Tang Z., Du D. & Lin Y. (2013). Graphene based materials for biomedical applications. *Materials Today, 16* (10), 365-373.

Yi H., Deng H., Tang X., Yu Q., Zhou X., Liu H. (2012). Adsorption equilibrium and kinetics for SO2, NO, CO2 on zeolites FAU and LTA. *Journal of Hazardous Materials, 203–204,* 111–117.

Yu H., Zhang B., Bulin C., Li R. & Xing R. (2016). High-efficient Synthesis of Graphene Oxide Based on Improved Hummers Method, *Scientific Reports, 6* (36143), 1-7.

Yusof N., Rana D., Ismail A. F.& Matsuura T. (2016). Original Microstructure of polyacrylonitrile-based activated carbon fibers preparedfrom solvent-free coagulation process, *Journal of Applied Research and Technology, 14* (1), 54–61.

Zhang P., Wanko H., Ulrich J. (2007). Adsorption of SO2 on activated carbon for low gas concentrations. *Chemical Engineering Technology, 30* (5), 635-641.

Zhao, J., Liu L. & Li F. (2015). *Graphene Oxide: Physics and Applications*. Springer.

Zheng Q. & Kim J. (2015). *Graphene for Transparent Conductors Synthesis, Properties and Applications.* New York: Springer.

CURRICULUM VITAE

Name Surname **:**Özge ALPTOĞA

Place and Date of Birth **:** İstanbul, 04.06.1993

E-Mail **:** ozgealptoga@hotmail.com

B.Sc. **:**2015, Yıldız Technical University, Faculty of Chemistry&Metallurgical, Chemical Engineering Department

PUBLICATIONS, PRESENTATIONSON THE THESIS:

- **Alptoğa Ö., Ucar N, Yavuz N. K. & Onen A.** 2017. Adsorption of SO_2 on metal-doped graphene oxide fibers; 16th International The Recent Progress Symposium on Textile Technology and Chemistry, May 4-6 2017 Bursa, Turkey.
- **Alptoğa Ö., Ucar N, Yavuz N. K. & Onen A.** 2017. Effect of the Coagulation Bath and Reduction Process on SO_2 Adsorption Capacity of Graphene Oxide Fiber, ICTETT 2017: 19th International Conference on Textile Engineering and Textile Testing, June 21-22 2017 Venice, Italy.
- **Ucar N., Olmez M., Alptoga Ö., Yavuz N. K. & Onen A.** 2016. Graphene Oxide Fiber with Different Exfoliation Time and Activated Carbon Particle, *World Academy Science Engineering and Technology*, 1514-1518,